



LIETUVOS
ENERGETIKOS
INSTITUTAS



Vilnius University
Institute of
Theoretical Physics
and Astronomy

Annual Report of the Association EURATOM / LEI

2009

ISSN 2029-1612

© Lithuanian Energy Institute, 2009

Content

1	Introduction	4
2	Accident analysis and evaluation of consequences for W7-X	5
2.1	Analysis of 40 mm pipe rupture during “baking” mode operation	6
2.2	Leak-before-break concept application to target	11
2.3	Modelling of the welds in plasma vessel	13
3	Atomic parameters for spectroscopic plasma diagnostics	16
3.1	New form of universal potential designed to solve quasirelativistic equations	16
3.2	Application of new quasirelativistic approach for investigation of highly-charged tungsten ions	20
3.3	Application of the quasirelativistic approach for investigation of W II ion. ...	22
3.4	Investigation of Auger cascades and relaxation effects following the production of a vacancy by electron impact in the tungsten W^+ , W^{3+} and W^{5+} ions	26
3.5	Relativistic electron-ion scattering calculation	28
3.6	Calculation of collision strengths for the W^{45+} ions using relativistic R-matrix code	30
3.7	Theoretical study of magnetic dipole transitions using Dirac-Fock approach	32
3.8	Properties of Auger electrons following excitation of polarized atoms by polarized electrons	34
3.9	Collaboration of VU ITPA with ADAS and JET	36
4	Mobility program 2009	37
5	Public information	39
6	Publications	40
7	Implementation of QA system	41
8	References	42

1 INTRODUCTION

Today, about 80% of all energy produced comes from the fossil fuel (oil, carbon, and natural gas). European scientists are developing environmentally friendly, safe, and renewable energy technologies. Nuclear fusion is one of them. Nuclear fusion reactors promise high power energy sources, which have low impact on environment, are safe and have virtually unlimited fuel resources. This technology is not limited to heat and electricity generation, it also could be used for hydrogen production, which would lead to further development of the “hydrogen economy”.

European nuclear fusion research program allows using common European research and their development resources in all important research areas. Co-operation is especially important not only in the operation of the Joint European Torus (JET), but also in the execution of the European Fusion Development Agreement (EFDA) technological program, which is devoted to the ITER project, and also encompasses promising DEMO research. European fusion research and development program, based on EURATOM contract, is being coordinated and carried out by the European Commission.

After negotiations took place in the year 2006, Lithuanian Energy Institute (LEI) signed a contract on joining the EFDA agreement. On 2006 November 15, the first meeting of this project with the participation of the European Commission and Lithuanian organizations took place. During this meeting, project execution rules were presented and work programs for the year 2007 were agreed. The signed contract came into force from 1st January 2007 and Lithuania has officially become an EFDA member.

Following signed contract, work program is composed every year and approved by the steering committee.

Currently, there are two Lithuanian organizations participating in the EFDA project – Lithuanian Energy Institute and Vilnius University Institute of Theoretical Physics and Astronomy. Information regarding works performed by both these institutions during the year 2009 is presented in this report.

2 ACCIDENT ANALYSIS AND EVALUATION OF CONSEQUENCES FOR W7-X

W7-X (Figure 2.1) is a stellarator type nuclear fusion experimental device, currently being built at the Max Planck Institute of Plasma Physics (Max-Planck-Institut für Plasmaphysik (IPP), in Greifswald, Germany. The purpose of this facility is to demonstrate that stellarator type devices can be used to sustain stable plasma conditions for half an hour and longer. Plasma diagnostics and control technologies would be tested in this facility. Protective plates and cooled components of first wall used inside the plasma torus are made from the same materials, which will be used for the ITER facility; therefore, W7-X will also contribute to the ITER development.

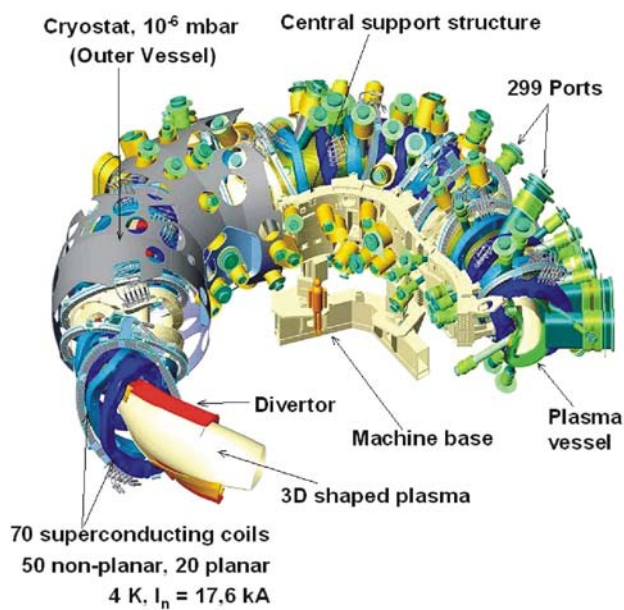


Figure 2.1

The fragment of a CAD model of the W7-X system

Co-operation between LEI and IPP started in the year 2007 and were continued during the year 2009. It was planned to update the developed models and perform detailed analysis of 40 mm diameter cooling water pipe rupture. In W7-X design a rupture of one 40 mm diameter pipe, providing water to the divertor target is the most severe accident in terms of vacuum vessel pressurization [1]. In order to avoid negative effects on device equipment absolute pressure inside the torus must not exceed 1.1 bar. To avoid the plasma vessel overpressure, active (safety valves on coolant pipes) and passive safety devices (burst or rupture disk) are used. The burst disk has to be opened at 1.1 bar pressure inside the torus and relief steam into the torus hall, i.e. room in which W7-X is situated. Steam can be released from the torus hall with the means of ventilation or through the safety valves. During one of the LEI and IPP meetings it was decided

that LEI will perform analysis of the 40 mm diameter pipe rupture during the W7-X operation mode “baking” and will also perform strength analysis of the 12 mm diameter pipe [2].

The first analyses were performed in 2008, which considered assumptions where the design information was missing regarding the lengths and diameter of the piping. In 2009 this information was updated and this new information is considered in the piping model for RELAP5 code. “Baking” mode of the device operation is used in order to preheat constructions of the torus and to clean the plasma vessel before plasma ignition. RELAP5 [3] and COCOSYS [4] program codes were used for the pipe rupture analysis. RELAP5 was used to obtain coolant flows in the coolant system piping and parameters of the coolant flowing through the rupture (mass flow rate and specific enthalpy). Information obtained from the RELAP5 code calculation was used further performing calculations with the COCOSYS program code, which is suitable to obtain evolutions of the thermodynamic parameters inside the plasma vessel and torus hall.

In 2009 there were released 3 reports on the performed analysis [5, 6, 7].

2.1 Analysis of 40 mm pipe rupture during “baking” mode operation

In Figure 2.2 there is shown a layout of the W7-X device cooling circuit and “baking” circuit. This scheme and other project information was analyzed and discussed with the IPP specialists. Information was later systematized and model of the piping system was developed for the RELAP5 computer code. The general scheme of the W7-X device cooling and “baking” circuits are shown in Figure 2.3. It was used performing the analysis of the 40 mm diameter pipe rupture. With the aim to analyse rupture of the pipe, one of the five modules was modelled in more details (Figure 2.4). In this module, target elements were separated and an assumption that the ruptured pipe was providing coolant for the upper 1TH element (model element “136”) was made. The rupture was simulated by making assumption that during the accident the valve “198” is opened and coolant flows into the volume, which is indicated as “199” in the model.

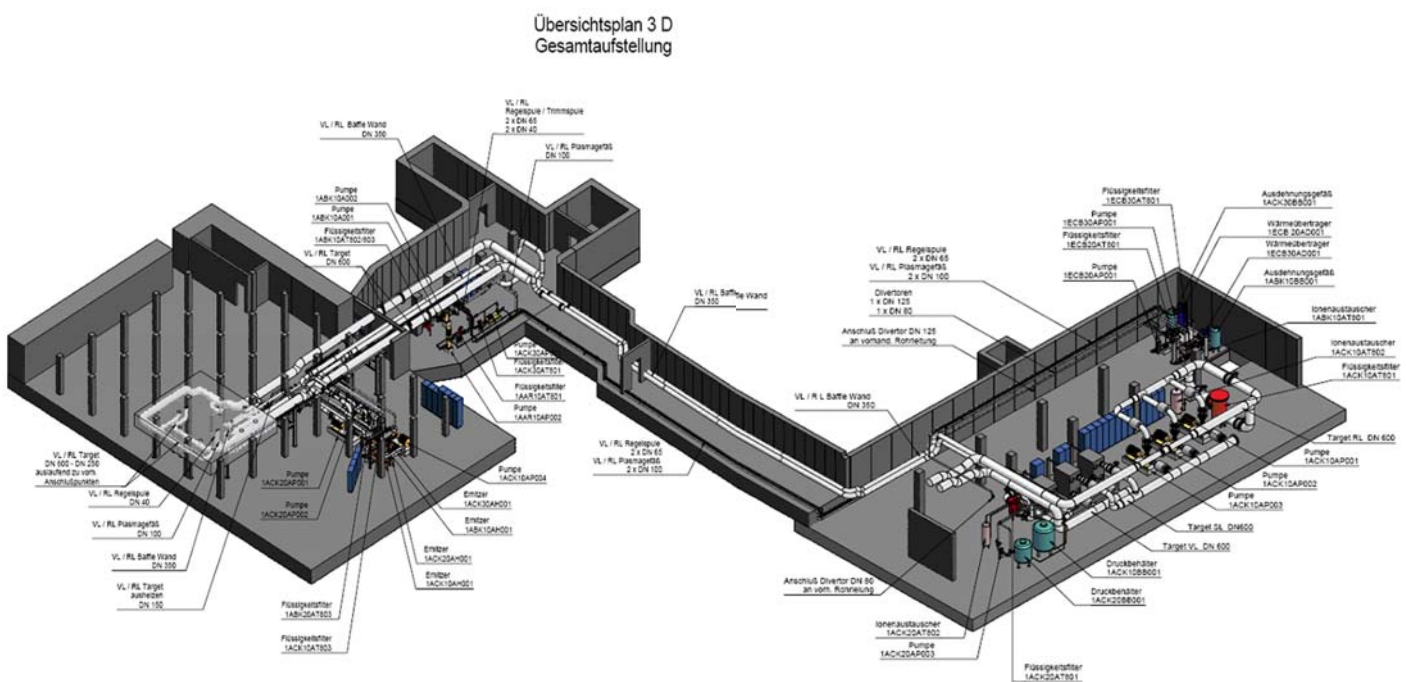


Figure 2.2
Layout of the W7-X device cooling circuit and “baking” circuit

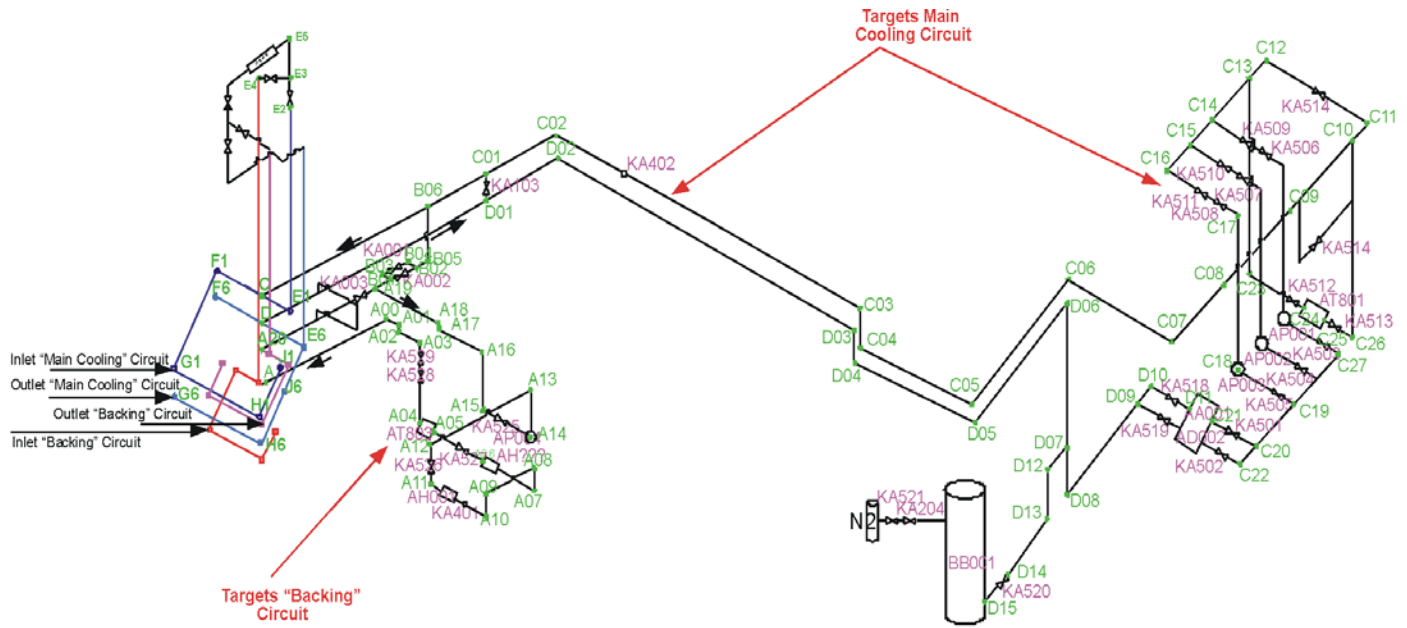


Figure 2.3
RELAP5 nodalisation scheme of the cooling and "baking" circuits

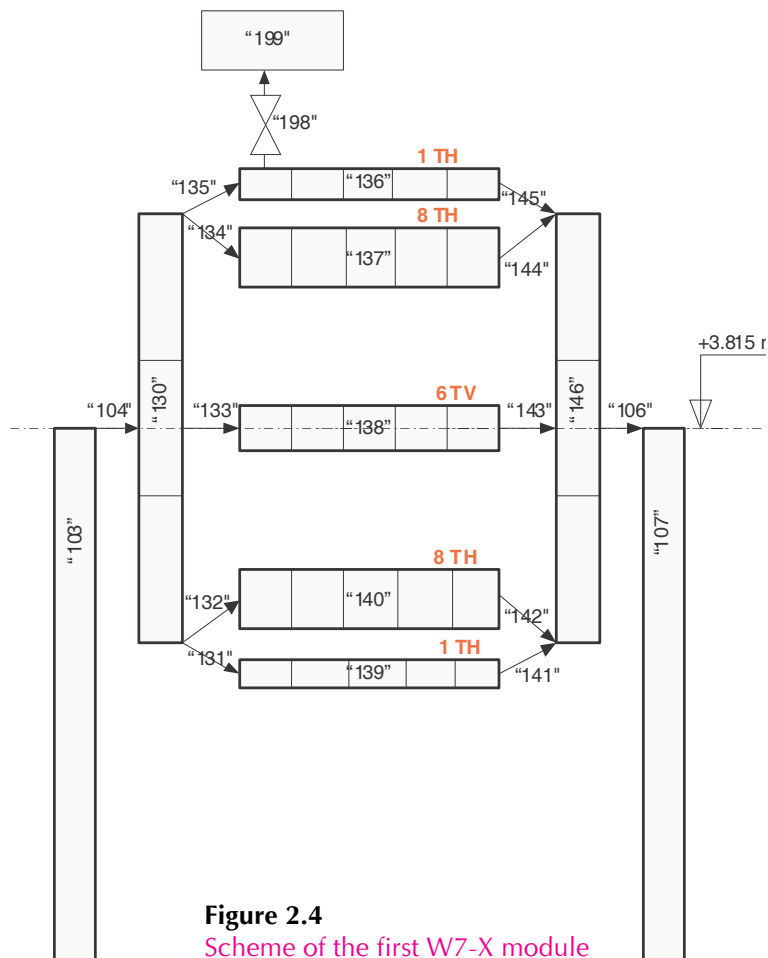


Figure 2.4
Scheme of the first W7-X module

Parameters of the cooling circuit during the "baking" regime were given in the project documentation as follows: pressure in the piping 10 bar, coolant temperature 160 °C, coolant flow in the piping – 1382 m³/hour (348 kg/s). Water flow in the "baking" circuit – 177 m³/hour (44.6 kg/s).

The following accident scenarios were considered for the analysis:

- Variant 1. Guillotine rupture of 400 mm diameter pipe connected to upper target. Automatic valves on inlet close when the pressure in plasma vessel increases to 2000 Pa. Pump in „baking” circuit trips when outlet pressure of pump reaches 1.8 MPa.
- Variant 2. Guillotine rupture of 400 mm diameter pipe connected to upper target. Automatic valves on inlet close when the pressure in plasma vessel increases to 2000 Pa. Pump in „baking” circuit trips when signal on closure of valves at the inlets to targets is generated.
- Variant 3. Same as Variant 2 but with small inertia of the pump.
- Variant 4. Same as Variant 1 but ruptures the pipe connected to the lower target.
- Variant 5. Same as Variant 2 but assuming that one of the automatic valves is not closed tightly i.e. there is a leakage through the valve.
- Variant 6. Same as Variant 4. Investigation of influence of plasma vessel modelling.

The analysis of consequences of 400 mm diameter pipe rupture are presented below. The water flow through the pump and the discharge of coolant through the rupture are presented in Figure 2.5.

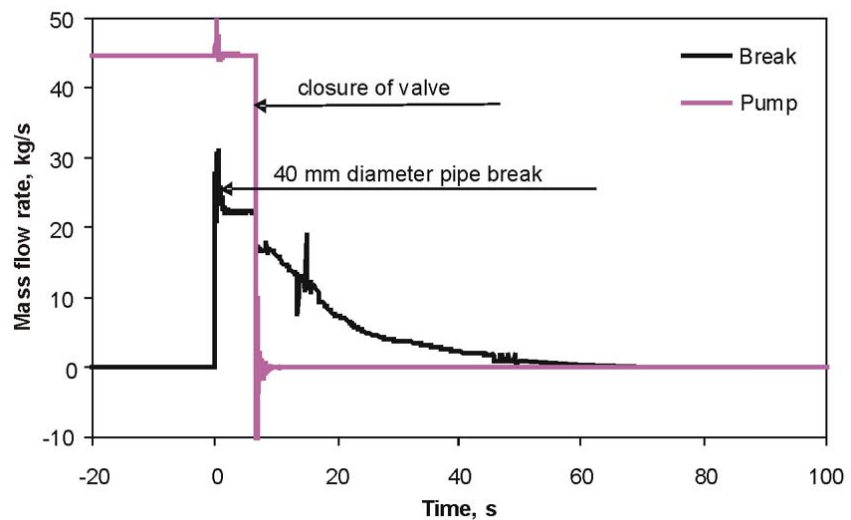
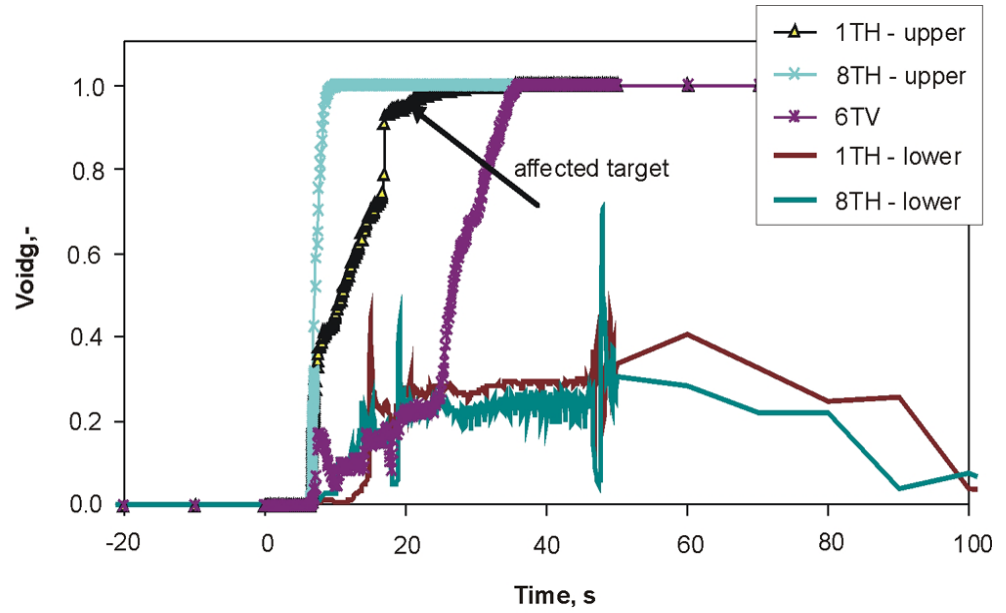


Figure 2.5
Flows of coolant through the pump and rupture pipe

It is assumed, that the accident starts at time moment $t = 0$ s. After the rupture of pipe the water is leaking through the rupture inside the plasma vessel. This leads to pressure increase in the plasma vessel. When pressure in plasma vessel reaches 2000 Pa safety system of W7-X facility generates signal to close automatic valves, which are in the inlet of targets modules. The trip of pump in „baking” circuit is generated according the same signal. After close of these automatic valves the water flow through the pump is stopped. Discharge of water through the break to the plasma vessel slightly decreases, because the water from other targets is discharged till pressure in the intact targets modules decreases down to the pressure in plasma vessel.

The behaviour of void fraction in the separate targets modules is presented in Figure 2.6. The upper target modules will be empty after approximately 7 s („8TH upper” curve), and only after 30 s the intact target module becomes empty („1TH upper” curve). This happens because the all target modules are connected together and water from intact targets modules discharged in the plasma vessel through the affected target. After 37 s water from vertical target modules („6TV” curve) also becomes empty, but still some water remains in the lower target modules.

Figure 2.6
Void fraction of the coolant in the different targets



The parameters of coolant, which is discharged through the rupture (flow and specific enthalpy) calculated using RELAP5 code are presented in Figure 2.7. These parameters are necessary for further calculation of processes in plasma vessel and torus hall.

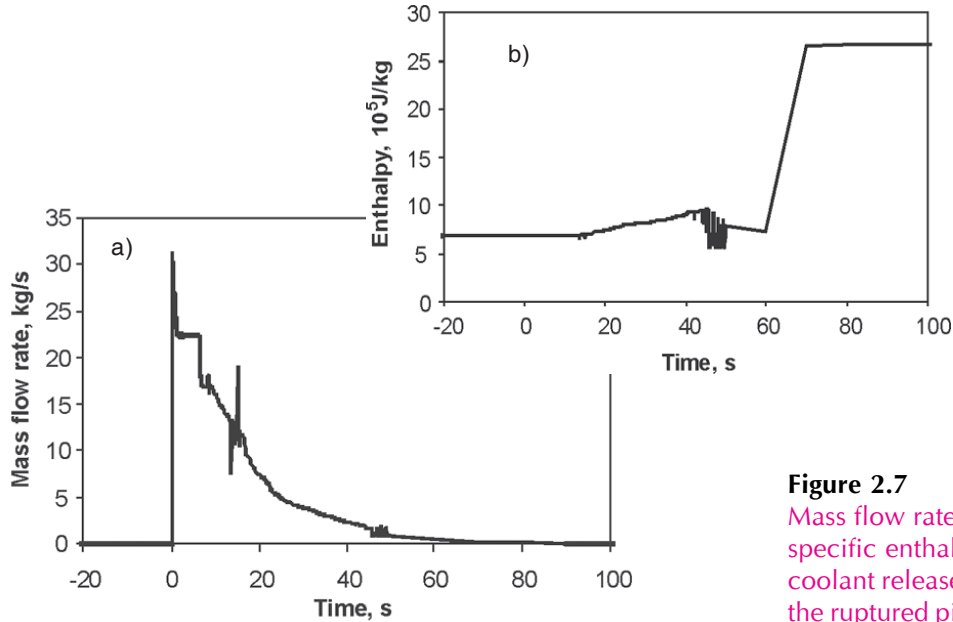


Figure 2.7
Mass flow rate and specific enthalpy of the coolant released through the ruptured pipe

The comparison of coolant flow rate through the 40 mm pipe rupture in upper and lower target modules is shown in Figure 2.8. Maximal coolant flow rate through the ruptured pipe reaches $\sim 30 \text{ kg/s}$ in both cases. After 2 s coolant flow rate through the rupture in lower target module is different comparing to rupture in upper target module. Calculation results shows that discharge of coolant is higher in case of lower target rupture. This is because position of the rupture is

lower, thus the water from all upper and vertical target modules are removing faster, comparing to rupture in upper target module. It is necessary to point out, that in the lower target rupture case - lower target modules becomes empty. Received calculation results shows that 40 mm pipe rupture in lower target module is more dangerous.

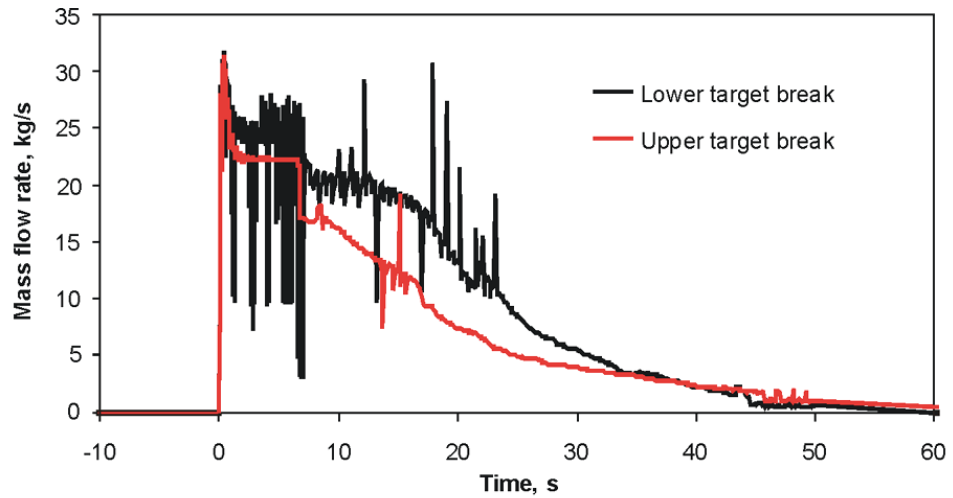


Figure 2.8
Coolant release to plasma vessel when rupture occurs in upper and lower targets

The discharge of coolant through the rupture in Variants 2 and 5 is compared in the Figure 2.9. The coolant leakage 1% and 10% of valve free cross-section flow area was assumed in Variant 5. This calculations was made for taking to assumption, that in case some failure the automatic valves did not close properly and leaves 1% and 10% of valve free cross-section area. As it is seen, the results of Variant 2 (all automatic valves are closed properly) and coolant leakage 1% from valve are similar – coolant flow rate through the rupture in both cases are close to each other. Calculation results with coolant leakage 10% free cross-section flow area from Variant 2 differs significant. Coolant flow rate through the brake after 10 s from event is significant bigger comparing to Variant 2 and coolant leakage 1% variant. After 100 s from event mass flow of coolant through the break still is about 6 kg/s (Figure 2.9) and this situation can lead to overpressure in plasma vessel.

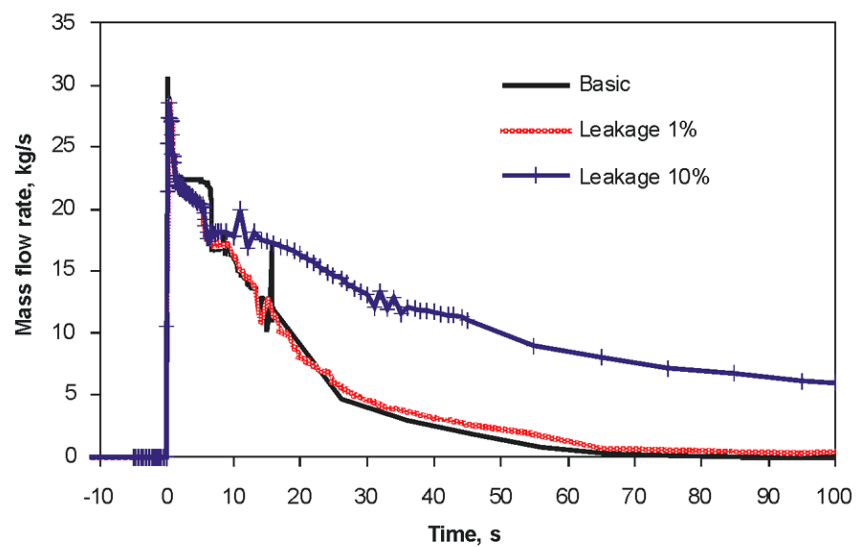


Figure 2.9
Coolant release to plasma vessel assuming different leakages of the valve

2.2 Leak before break concept application to target

The aim of deterministic Leak-Before-Break (LBB) analysis is to calculate the maximum acceptable leak rate through postulated cracks and if possible to detect this leakage during acceptable time by existing leak monitoring systems. The leak before break analysis of the pipe of upper part of the target module 1H (see Figure 2.10) was performed at 2009. The place of installation of this target module (red colour) in the plasma vessel is presented in Figure 2.11.

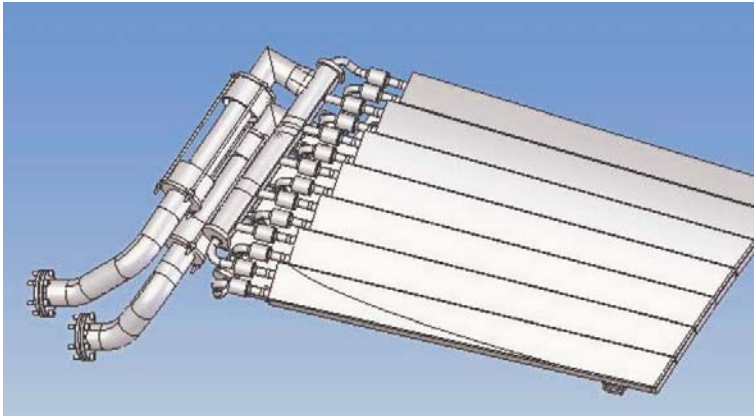


Figure 2.10
Model of the Target module 1H

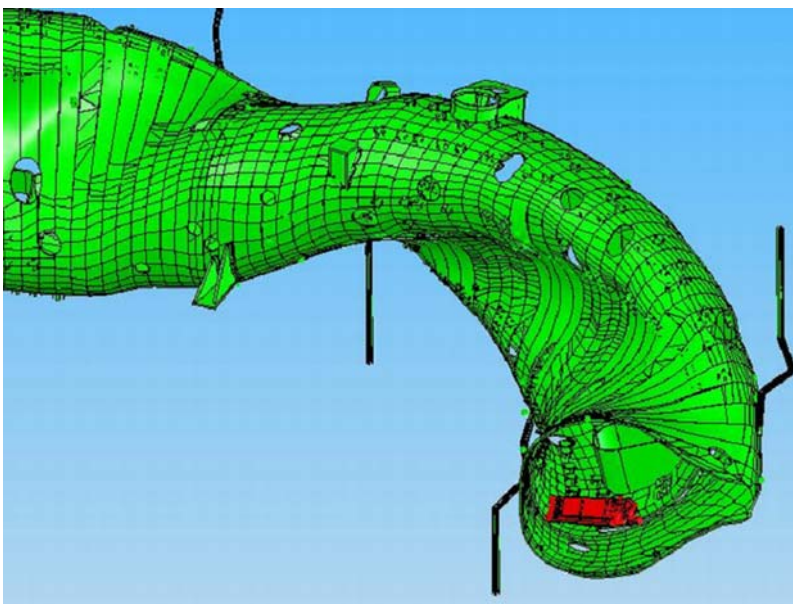


Figure 2.11
Location of target (red element)
in the plasma vessel

The place of the target module 1H pipe, in which was modelled through-wall crack, was selected according stress analysis results. The finite element model of this target module was prepared. The stress analysis was carried out using prepared model (Figure 2.12) and the most loaded zone of this target module was selected. This analysis is only for selection most loaded place and is not detailed analysis of strength. Pipe selected for LBB analysis is presented in Figure 2.12.

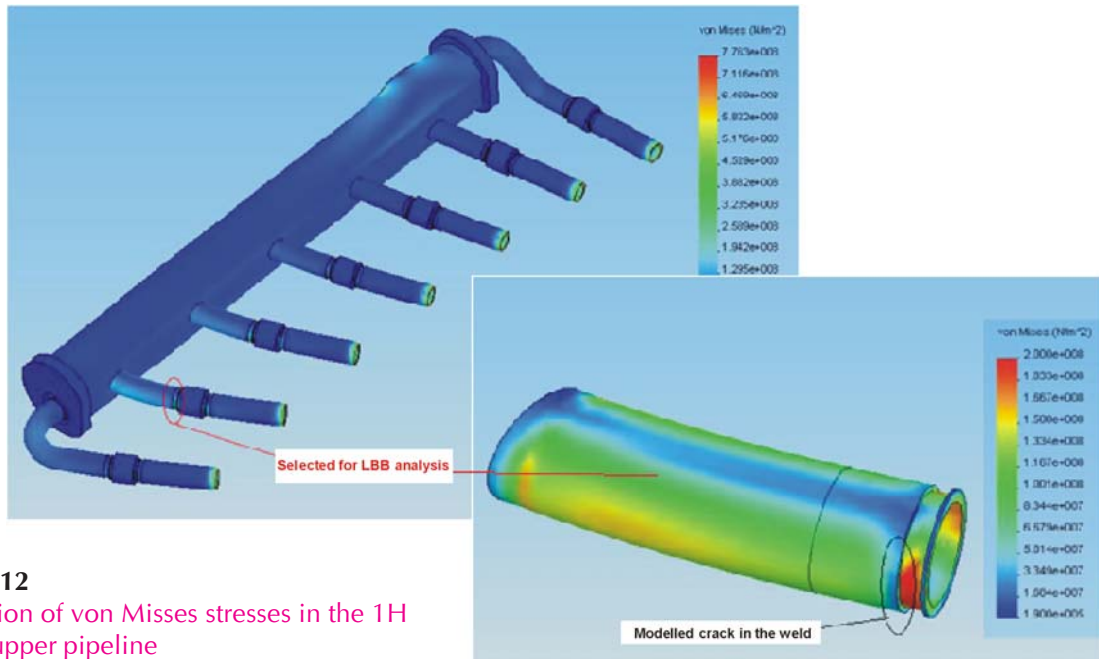


Figure 2.12
Distribution of von Mises stresses in the 1H module upper pipeline

The analysis of the critical and acceptable crack sizes was based on engineering safety assessment procedure R6. The finite element model of target module with through-wall crack (Figure 2.13) was developed using finite element software CASTEM 2000 and the function of crack opening was calculated.

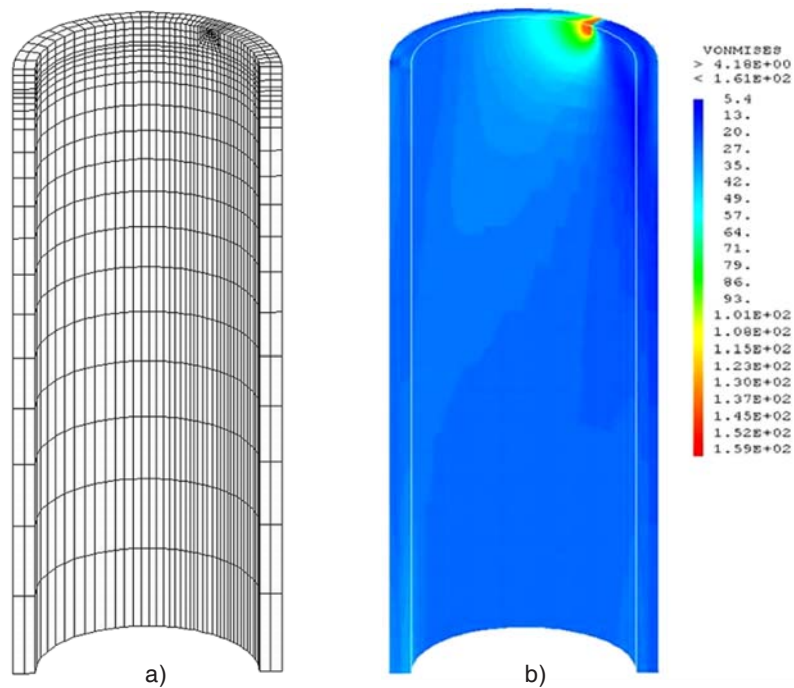


Figure 2.13
FE model of pipe of inner diameter 10 mm with through-wall crack (a) and Von Mises stress distribution

The leak rate through the crack is calculated using the computer program SQUIRT v.2.4. The received analysis results show that the small leak will be in case of the small crack size (Figure 2.14). The vacuum environment is inside of the plasma vessel and this leakage inside of the plasma vessel will be detected immediately. The guillotine failure of pipe can be when crack size exceeds the critical through-wall crack size (6.5 mm) and the leak rate through this crack will be 1.4 kg/h.

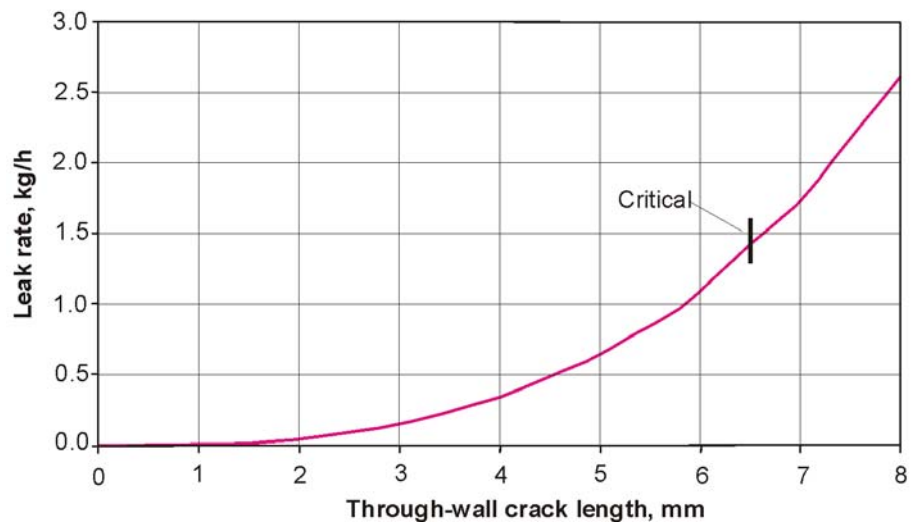


Figure 2.14
Variation of crack opening displacement with crack length

The degradation mechanisms of the target module 1H at influence of the magnetic field and the stress corrosion cracking was evaluated in this analysis. According the received results was determined that the through-wall crack will be reached after $2.8 \cdot 10^4$ cycles affected by the magnetic field and after 6 years operation in case of the stress corrosion cracking. According operation condition of W7-X machine the results of the analysis are conservatives. Also the probability of developing the through-wall crack is very small.

LBB analysis demonstrate that in case of developing through-wall crack, and some amount of coolant will flow through this crack, and this leakage will be detected immediately because the vacuum environment is inside of the plasma vessel, and the through-wall crack size remains stable, i.e. the guillotine failure of pipe of the target module 1H will not occur.

2.3 Modelling of the welds in plasma vessel

The models of the port welds between the plasma vessel and the ports in W7-X cryostat system was prepared using software's SolidWorks and Brigade/Plus. Software SolidWoks was used for preparing the geometrical models of these port welds. The geometrical models of the port welds between the plasma vessel and the port are presented in Figure 2.15 and Figure 2.18. The geometrical models of the port welds and the plasma vessel around it was transferred to finite element software Brigade/Plus. The finite element (FE) models of these port welds was prepared using software Brigade/Plus (see Figure 2.16 and Figure 2.19). The test analysis of these FE models was carried out. Results of these analyses are presented in Figure 2.17 and Figure 2.20.

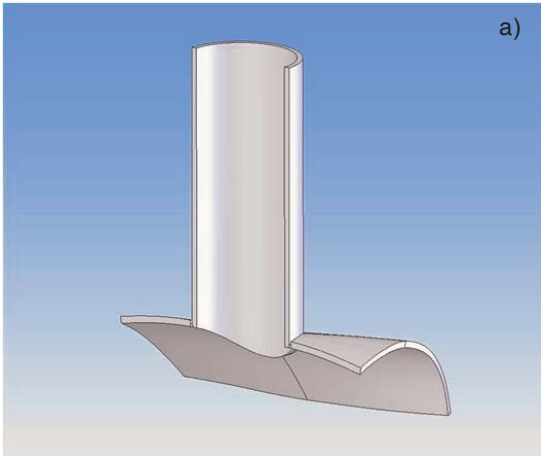


Figure 2.15
Geometrical model of port weld AEU30 between the plasma vessel and the port

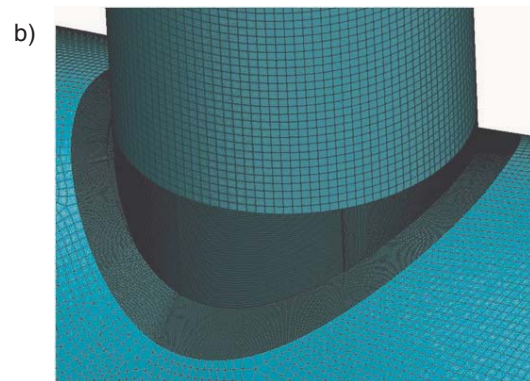
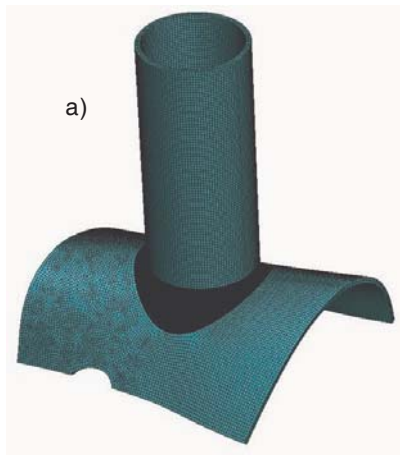
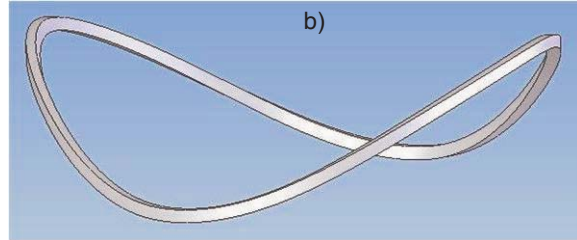


Figure 2.16
FE model of port weld AEU30 between the plasma vessel and the port

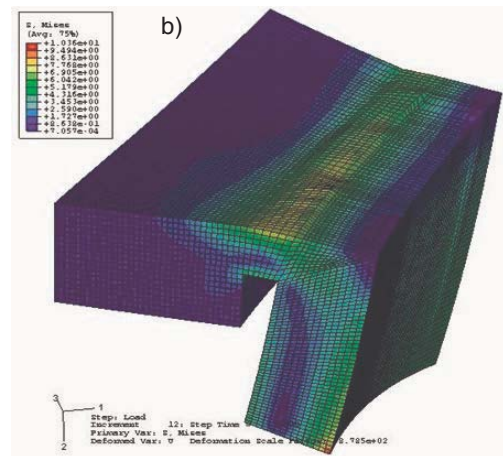
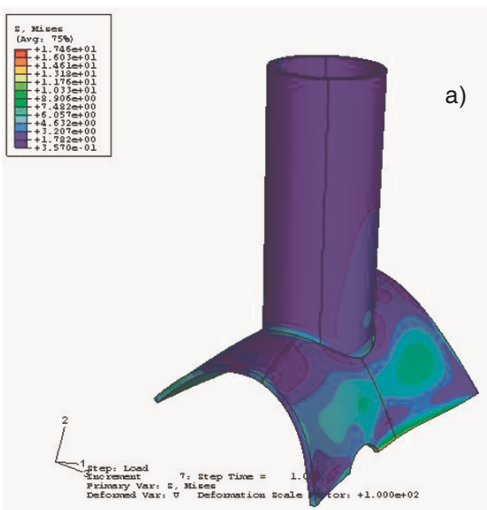


Figure 2.17
Test analysis results of the port weld AEU30 between the plasma vessel and the port

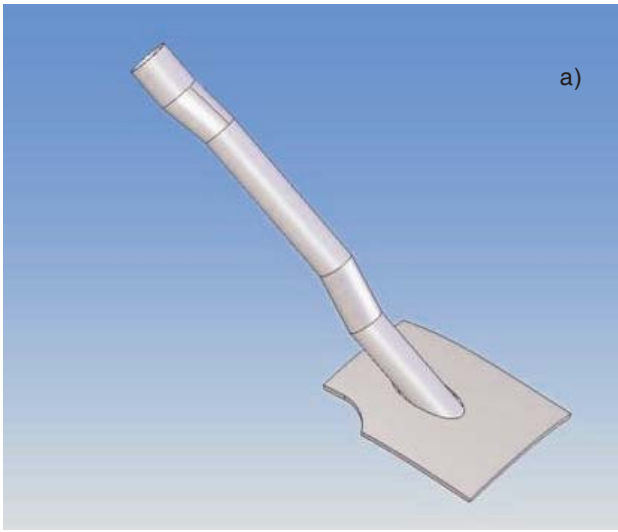


Figure 2.18
Geometrical model of port weld
AEQ20 between the plasma vessel
and the port

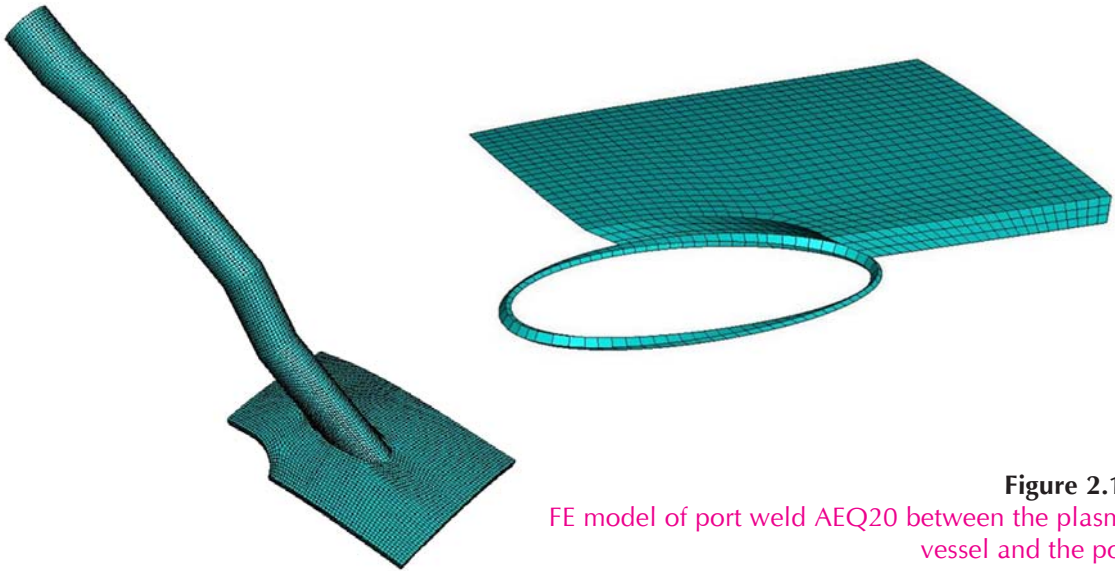
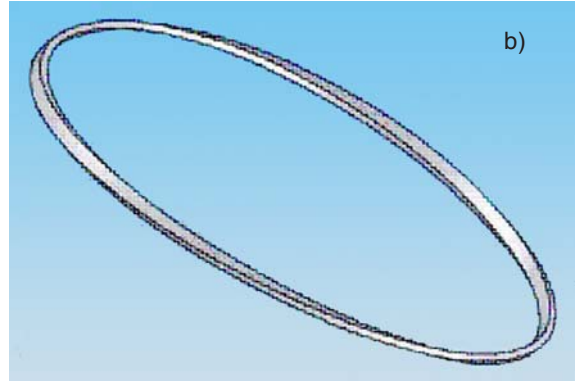


Figure 2.19
FE model of port weld AEQ20 between the plasma
vessel and the port

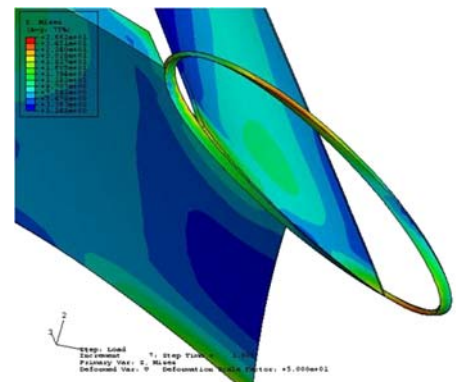
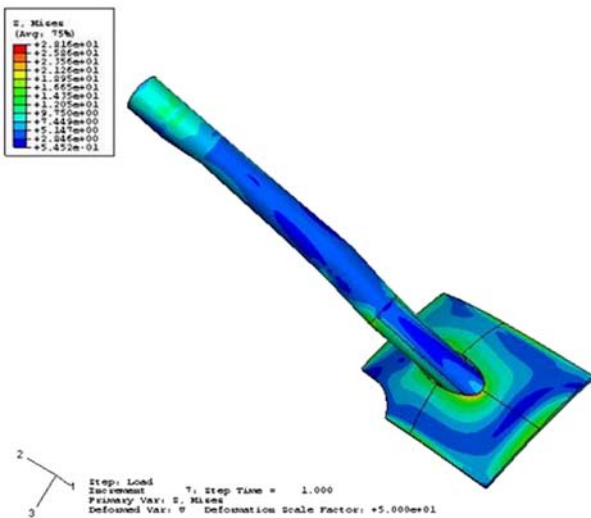


Figure 2.20
Test analysis results of the port weld AEQ20
between the plasma vessel and the port

3 ATOMIC PARAMETERS FOR SPECTROSCOPIC PLASMA DIAGNOSTICS

The ambitious goal to employ fusion reactions for energy production requires using of deuterium-tritium mixture as a fuel at the modern level of technology. Tritium operations in fusion reactors put in new claims for plasma facing materials. As tritium is a radioactive element, its retention inside a fusion device becomes one of the main issues in this research field besides more traditional ones, such as resistance to heavy heat and neutron irradiation, reduction of dust production. In this perspective exploitation of high-Z materials, namely tungsten, in some parts of a fusion device is treated as a solution for mentioned tasks. Tungsten is known as a heat-resistant matter. Usage of tungsten as a plasma-facing material resolves the tritium retention issue but it brings new challenges in implementation of high-performance long-lasting fusion devices needed for energy production. If tungsten or another high-Z element is detached from the wall and penetrates into the thermonuclear plasma it irradiates strongly thus cooling the plasma. It is necessary to ensure that inner walls of the reactor last for rather long period of time reasonable for industrial and not only experimental exploitation. Thus tungsten abundance inside the thermonuclear reactor must be carefully controlled. For this purpose relevant spectroscopic data on characteristics of various tungsten ions is necessary. Unfortunately the spectra of majority of these ions are very complicated and in many cases they form quasi-continuum or emission bands. So both the experimental and theoretical investigation of spectral properties of tungsten ions is a complex task still far from completion.

3.1 New form of universal potential designed to solve quasirelativistic equations

One of the main tasks for this year was to apply the created quasirelativistic approach for investigation of the highly-charged tungsten ions. While applying the approach it has been revealed that some difficulties occur solving the quasirelativistic Hartree-Fock equations described in [14, 15]. The equations are solved numerically by iteration. In order to start the iteration process one needs to have initial radial orbitals. In the case of usual Hartree-Fock equations [16] the universal Gaspar potential [17 – 19] of a simple analytic form

$$U_G(r) = -\frac{I}{r} - \frac{1}{r}(Z-I) \frac{e^{-B_0 Z^{1/3} r}}{1 + A_0 Z^{1/3} r} \quad (1)$$

is used. Here r – radial variable, Z – nucleus charge, I – ionization degree in spectroscopic notation ($I = 1$) for neutral atoms). The numerical values of the parameters of the potential are the following:

$$A_0 = 1.19, \quad B_0 = 0.2075. \quad (2)$$

The same potential was used to obtain the initial radial orbitals for solving the quasirelativistic Hartree-Fock equations.

Unlike within the non-relativistic approach, the initial radial orbitals using this potential obtained are not accurate enough for the quasirelativistic equations. By this reason not only the iteration process is elongated but also it is impossible to solve the quasirelativistic equations some times especially in the case of highly-charged ions. To solve the problem the decision has been made

to modify the universal potential employed by adjusting the values of the parameters without any changes of the form of the potential. The quasirelativistic radial orbitals were obtained for the ground configurations of 5 to 86 electrons to achieve the goal. The radial orbitals were calculated starting with neutral atoms and down to the highly-charged ions with a nucleus charge equal to 100. Some difficulties occurred while solving the quasirelativistic Hartree-Fock equations for these ions. In many cases we had to adjust the parameters of the universal potential in order complete the iteration process successfully. Unfortunately there were a whole series of ions when solutions had not been obtained. Nevertheless a total number of ions for which the equations were successfully solved exceed 360. The numbers of electrons of all investigated configurations and the nucleus charges are listed in Table 3.1.

A direct potential U_{QR} of most outer electron was calculated for each of these configurations. Further this potential was approximated by the formula (1) choosing the values of the parameters $A_{Z,l}$ and $B_{Z,l}$ for each configuration by least squares method. When all the values of the parameters had been obtained the dependences on the values of the nucleus charge were found for every isoelectronic sequence expressing A_N and B_N through the degrees of ionization

$$A_N(l) = a_{N,0} + a_{N,1}l + a_{N,2}l^2; \quad B_N(l) = b_{N,0} + b_{N,1}l + b_{N,2}l^2. \quad (3)$$

The fitting of the expansion coefficients from (3) was performed by parabolas reflecting their dependence on the number of electrons within the configuration:

$$a_{N,k} = \alpha_{0,k} + \alpha_{1,k}N + \alpha_{2,k}N^2; \quad b_{N,k} = \beta_{0,k} + \beta_{1,k}N + \beta_{2,k}N^2. \quad (4)$$

The numerical values of the coefficients α and β were obtained by the least squares methods as before. Thus the following analytical expressions were obtained for the parameters of the universal potential:

$$\begin{aligned} A(N, l) = & 168292295 - 1.54855956 \cdot 10^{-2} \cdot N + 1.18613040 \cdot 10^{-4} \cdot N^2 \\ & + l \cdot (6.80267876 \cdot 10^{-2} - 1.95268774 \cdot 10^{-3} \cdot N + 1.79791804 \cdot 10^{-5} \cdot N^2) \\ & + l^2 \cdot (5.62961892 \cdot 10^{-4} - 1.42822397 \cdot 10^{-5} \cdot N + 4.29849376 \cdot 10^{-8} \cdot N^2) \end{aligned} \quad (5)$$

Table 3.1. Numbers of electrons of all investigated configurations (N) and nucleus charges (Z)

N	Z
5	5 - 13, 15, 17, 20, 25, 30, 45, 50, 55, 60, 70, 80, 90
6	6 - 16, 18, 20, 22, 24, 26, 28, 30, 32, 35, 37, 40, 45, 50, 55, 60, 70, 80, 90
8	8 - 20, 22, 24, 26, 28, 30, 32, 35, 37, 40, 45, 50, 55, 60, 70, 80, 90
10	10 - 18, 20, 22, 24, 26, 28, 30, 32, 35, 37, 40, 45, 50, 55, 60, 70, 80, 90
19	21 - 27, 29, 30, 32, 35, 37, 47, 50, 55, 60, 70, 80, 90
37	37 - 45, 47, 48, 49, 50, 52, 60, 62, 65, 67, 70, 80, 90
47	47 - 55, 60, 62, 65, 67, 70, 75, 80, 85, 90, 95
54	54 - 64, 66, 68, 70, 72, 74, 76, 78, 82, 84, 85, 90, 100
68	68 - 75, 77, 80, 83, 85, 87, 90, 95, 100
70	70 - 80, 82, 84, 86, 88, 90, 92, 95, 97
80	80 - 100
86	86 - 100

$$\begin{aligned}
B(N, I) = & 0.253862830 - 1.93417591 \cdot 10^{-3} \cdot N + 1.81755849 \cdot 10^{-5} \cdot N^2 \\
& + I \cdot (9.43884981 \cdot 10^{-2} - 2.50023623 \cdot 10^{-3} \cdot N + 1.77429131 \cdot 10^{-5} \cdot N^2) \\
& + I^2 \cdot (-4.73906019 \cdot 10^{-4} + 1.22191182 \cdot 10^{-5} \cdot N - 7.41630927 \cdot 10^{-8} \cdot N^2).
\end{aligned} \tag{6}$$

The described procedure was repeated approximating not the direct potential itself, but the effective charge

$$q(r) = -I - (Z - I) \frac{e^{-B_0 Z^{1/3} r}}{1 + A_0 Z^{1/3} r} \tag{7}$$

that creates the potential. In this case the following values of the parameters of the universal potential (1) were obtained:

$$\begin{aligned}
A^q(N, I) = & 1.09270806 - 5.08422790 \cdot 10^{-3} \cdot N + 7.29722952 \cdot 10^{-5} \cdot N^2 \\
& + I \cdot (5.26634851 \cdot 10^{-2} - 2.02788199 \cdot 10^{-3} \cdot N + 1.61348845 \cdot 10^{-5} \cdot N^2) \\
& + I^2 \cdot (3.16546385 \cdot 10^{-4} - 1.17222742 \cdot 10^{-5} \cdot N + 1.50926909 \cdot 10^{-7} \cdot N^2),
\end{aligned} \tag{8}$$

$$\begin{aligned}
B^q(N, I) = & 0.530964547 - 7.21449090 \cdot 10^{-3} \cdot N + 4.39624106 \cdot 10^{-5} \cdot N^2 + \\
& + I \cdot (0.108641267 - 2.52982224 \cdot 10^{-3} \cdot N + 1.82931326 \cdot 10^{-5} \cdot N^2) + \\
& + I^2 \cdot (-3.83202815 \cdot 10^{-4} + 1.05096094 \cdot 10^{-5} \cdot N - 1.05488797 \cdot 10^{-7} \cdot N^2).
\end{aligned} \tag{9}$$

Thus two new expressions of the universal potential were obtained. Here the parameters are not constants but functions of the degree of ionization and of the number of electrons within the configuration. These potentials were denoted U_N and U_N^q correspondingly. The validity of the potentials was verified by calculations. In Figure 3.1 three potentials are plotted: the direct potential obtained by solving the equations U_{QR} , the universal Gaspar potential U_G (1), and a new universal potential U_N .

As it is seen from the Figure 3.1 a new potential is in better agreement with the direct one. The potential U_N^q is not plotted in the Figure 3.1 since it merges with the potential U_N . Same picture were obtained in all other cases as well.

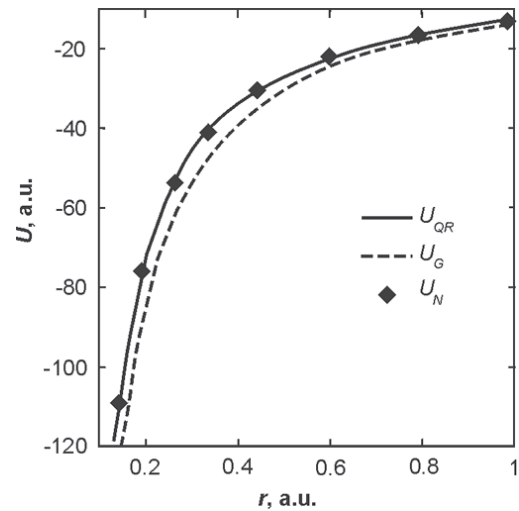


Figure 3.1
 U_{QR} , U_G , and U_N potentials for Ti XV ($Z = 22$)
ion of the oxygen isoelectronic sequence

The properties of the radial orbitals obtained using the new potentials were compared in order to prove the validity of potentials. One example of such comparison is presented in Table 3.2. In this table the single-electron energies of electrons obtained using three different types of the universal potential are compared with the values derived solving the quasirelativistic Hartree-Fock equations. The mean square deviations from the last values are presented at the end of Table 3.2. As it is seen from this the new potentials enable one to improve the accuracy of the single-electron energies of the initial radial orbitals. The same improvement is observed in all other cases both for the single-electron energies and for other characteristics of radial orbitals.

Table 3.2. Single-electron energies of the tungsten isoelectronic sequence

<i>nl</i>	<i>Z</i>	ϵ_{nl}			
		U_{QR}	U_G	U_N	U_N^q
1s	80	3080.04	3125.47	3074.08	3107.95
	90	4074.08	4187.37	4068.81	4124.66
2s	80	554.34	574.69	540.57	557.03
	90	770.93	837.67	756.76	783.78
2p	80	483.90	513.10	477.06	495.33
	90	658.58	742.05	657.30	687.01
3s	80	136.86	146.63	128.36	132.06
	90	204.70	242.73	197.75	203.38
3p	80	115.84	127.70	109.16	113.09
	90	172.40	214.20	168.83	174.70
3d	80	91.30	102.39	82.93	87.22
	90	138.55	178.77	131.63	137.79
4s	80	34.31	40.88	32.65	31.68
	90	61.40	83.64	61.85	60.01
4p	80	27.19	34.18	26.27	25.28
	90	50.47	73.12	52.04	50.21
4d	80	18.01	24.76	17.30	16.19
	90	37.64	59.29	38.96	36.93
4f	80	8.03	14.84	8.12	6.49
	90	24.49	46.66	26.72	23.72
5s	80	8.59	12.01	8.96	7.89
	90	22.00	33.14	23.64	21.75
5p	80	6.42	9.69	6.98	6.04
	90	18.24	28.95	20.13	18.43
5d	80	3.86	6.47	4.33	3.61
	90	13.87	23.30	15.41	13.95
6s	80	2.86	4.17	3.25	2.90
	90	10.41	15.42	11.51	10.72
σ	80		46.9	6.2	10.0
	90		55.2	6.5	2.2

Exploitation of the new universal potentials within the computer program for solution of the quasirelativistic Hartree-Fock equations ensures good convergence of the iteration process in

all cases starting with neutral atoms and down to the ions of ionization degree approaching 100. Origination of the new potentials and analysis of their properties is described in details in [20].

3.2 Application of new quasirelativistic approach for investigation of highly-charged tungsten ions

Tungsten ions of various degrees of ionization occur in the thermonuclear plasma and the ions with open 4d-shell are among them. These ions are namely W^{29+} to W^{37+} . In the spectra of so highly ionized atoms the relativistic effects play an important role. Thus there is a task occurred to check whether the new quasirelativistic approach (QR) [14, 15, 21] is suitable for investigation of the mentioned ions. As indicated in monograph [22] the quasirelativistic approach is characterized by facts that main relativistic effects are taken into account already when calculating the radial orbitals and the energy spectra is calculated within the Breit-Pauli approach similar as in the case of non-relativistic functions. Within the usual Breit-Pauli approach (BP) non-relativistic radial orbitals are used and the relativistic effects are taken into account in the energy operator to the square of the fine-structure constant. The most complete approach to take into account the relativistic effects is Dirac-Fock one (DF) but application of this approach is rather complicated compare to BP. On the other hand it is much easier to calculate the correlation corrections within QR approach. Thus it was necessary to examine if the QR results are in good agreement with DF data for the mentioned highly-charged tungsten ions.

The energy spectra and transition characteristics were calculated for the tungsten ions of configurations $4p^64d^N$ and $4p^64d^{N-1}4f + 4p^54d^{N+1}$ for N values from 2 to 9. The calculations were performed within three approaches: BP, QR, and DF. Since the goal of the research was to investigate the relativistic effects, the correlation effects were not taken into account. However, during the calculations the interaction between $4p^64d^{N-1}4f$ and $4p^54d^{N+1}$ configurations was included. As mentioned in [23] the energy spectra of these configurations are overlapping strongly for the tungsten ions under investigation. Thus it is impossible to obtain reliable results without taking into account this configuration interaction.

The tungsten ions under investigation are not sufficiently explored experimentally [24]. Due to it the calculated results were mostly compared with the results of the relativistic DF approach. In Table 3.3 the mean square deviations and the mean square relative deviations of the energy spectra of all investigated configurations calculated within BP and QR approaches from corresponding DF spectra.

Table 3.3. Mean square deviations σ (cm^{-1}) and mean square relative deviations S (%) of the energy spectra

<i>Method</i>		W^{+29}	W^{+30}	W^{+31}	W^{+32}	W^{+33}	W^{+34}	W^{+35}	W^{+36}
BP	σ	32100	30000	25200	29100	34965	46400	59200	71400
	S	1.89%	1.71%	1.55%	1.48%	1.58%	1.94%	2.50%	3.09%
QR	σ	13700	10900	9800	9000	8700	8900	9000	9600
	S	0.73%	0.69%	0.61%	0.51%	0.46%	0.44%	0.47%	0.53%

As it is seen from Table 3.3 the transition from the non-relativistic radial orbitals (BP) to the quasirelativistic ones (QR) allows to decrease several times both the mean square and the mean square relative deviations. It is important that the relative deviations of QR are decreasing almost constantly while ionization degree grows. At the same time both absolute and relative deviations of BP grow obviously. One must notice that QR approach provides with the same positions of the energy levels as DF approach. The difference is only for the energy levels of the excited configurations that appear slightly higher within QR approach than they are within DF

approach. At the same time the deviations of BP approach from DF one not only large by their absolute values but also they change their signs randomly thus a big number of levels are positioned in different order that they are in the relativistic energy spectra.

There is only one rather complete energy spectrum of $4d^2$ configuration of W^{36+} published in [24]. In Table 3.4 the theoretical results are compared to this experimental spectrum. The mean square deviations from the experimental spectrum are presented at the end of Table 3.4.

Table 3.4. Energy spectrum of $4d^2$ configuration of W^{36+} (cm^{-1})

LSJ	exp.[19]	BP	QR	DHF
3F_2	0	0	0	0
3P_0	67780	69210	69960	70560
3F_3	141310	134490	139040	139300
3P_2	174130	168440	173300	173600
1G_4	182760	178430	182960	183320
3P_1	184610	179970	185090	185380
3F_4	308530	298150	307030	307620
1D_2	331480	320820	330420	330890
1S_0	407000*	402050	411800	411880
σ		7130	1450	1290

* Calculated in [19] by fitting using Cowan codes.

As it is seen from Table 3.4 the transition from BP to QR improves the coincidence of the calculated results to the experimental ones. At the same time the value σ_{QR} is very close to σ_{DF} . Since the difference between these two values is much smaller than the mean value of the deviations one can state that further improvements of the accuracy of the energy spectra within QR approach can be reached not taking into account the relativistic effects more precisely but including the correlation effects into the calculations of the energy spectra.

The same conclusion appears while comparing the wavelengths and other transition characteristics. There are five experimental wavelengths of the transitions between investigated configurations presented in [24]. In Table 3.5 they are compared with the theoretical wavelengths. The probabilities of the emission transitions are presented there as well. As it is seen from the table the wavelengths QR and DF are in good agreement and are much more accurate than BP ones as one could expect. Same as for the energy spectra the differences between the QR and DF wavelengths are much smaller than their deviations from the experimental data. It is extremely important that the transition probabilities calculated by QR and DF approaches differ only slightly. This tendency is observed for almost all strong transitions between the investigated configurations. The approach used and the results obtained are described in details in [25].

Table 3.5. Characteristics of $4d^N - 4d^{N-1}4f$ transition

Ion	Final	Initial	λ (\AA)				A (10^{12}s^{-1})		
			exp.[19]	BP	QR	DF	BP	QR	DF
W^{+29}	$4d^9\ ^2D_{5/2}$	$4d^8(^3F)4f\ ^2F_{7/2}$	49.78	47.73	48.35	48.42	5.96	5.72	5.76
		$4d^8(^1G)4f\ ^2P_{3/2}$	49.94	48.12	48.52	48.63	6.09	5.93	5.97
		$4d^8(^3F)4f\ ^2D_{5/2}$	50.26	48.10	48.67	48.76	5.33	5.13	5.15
	$4d^9\ ^2D_{3/2}$	$4d^8(^3F)4f\ ^2F_{5/2}$	49.86	47.83	48.42	48.51	5.90	5.67	5.70
W^{+29}	$4d^2\ ^3F_2$	$4d4f\ ^3G_3$	54.14	52.86	53.03	53.19	2.59	2.77	2.73

The performed investigation revealed that the created quasirelativistic approach allows one to take into account the relativistic effects for tungsten ions with the filling 4d-shell. Further improvement of the results is connected with the inclusion of the correlation effects into the calculations. The obtained results allow expecting that the created quasirelativistic approach is suitable for calculations of the properties of the highly-charged ions as well.

3.3 Application of the quasirelativistic approach for investigation of W II ion

New quasirelativistic approach [14, 15, 21] was successfully applied for investigation of W II ion. Knowledge on spectral characteristics of first tungsten ions is important for monitoring and modeling of tungsten deposition inside the thermonuclear reactor when the atoms are detached from the wall but return back to it quickly without penetrating into the core of the plasma. During this process first tungsten ions can form and be registered by spectroscopic monitoring systems.

Earlier there was an attempt to perform *ab initio* calculations of the energy spectra of W II ion using the configuration superposition method on the basis of the non-relativistic radial orbitals but the obtained ground level was different than the experimental one. Thus in order to obtain the energy spectra and transition characteristics of W II the configuration superposition method on the basis of the transformed quasirelativistic radial orbitals was applied and preliminary calculations were performed.

The solutions of the quasirelativistic Hartree-Fock equations [14] were used to describe the configurations under research. The electrons of the admixed configurations with $n d'' 5$, $l d'' 3$ and $6s, 6p, 6d$ ones were described using the quasirelativistic radial orbitals and the electrons with $n e'' 7$ and $l d'' 7$ were described by the transformed quasirelativistic radial orbitals [21], which had been successfully applied in investigations of other heavy ions [26].

The investigated configurations were grouped according to their parity. This approach allows one to take into account the interactions between the configurations under research and that is extremely important in this case since the energies of the configurations of the same parity are very close to each other. The group of even parity configurations consists of the ground configuration $5d^4 6s$ and two excited ones $5d^5, 5d^3 6s^2$; the group of odd configurations is made of $5d^4 6p, 5d^3 6s 6p$ and $5d^2 6s^2 6p$. These configurations were chosen for investigation as the preliminary calculations performed on the small basis of radial orbitals had revealed that higher excited configurations are energetically distant from the investigated ones and their influence is rather weak.

The list of the admixed configurations was created for each group separately within the available basis of radial orbitals. The admixed configurations are formed by virtual excitations of one or two electrons from the 5d- and 6l-shells to the already existing shells or to the new ones described by the transformed quasirelativistic radial orbitals. The number of the admixed configurations obtained in this way is very large, but not all configurations are important for the calculation. Necessary admixed configurations are selected using SELECTCONF computer code [27]. In present calculation there were 714 admixed configurations selected for the even configuration group and 871 – for the odd group, using the selection parameter set to 10^{-8} . For this number of the admixed configurations the number of the generated terms (CSF) is extremely large: 369706 for even configurations and 730083 for odd ones. The computer program ATOTERM [28] was used to reduce these numbers of CSF to 79943 and 17541 correspondingly, that is more than four times. The multiconfiguration wave-functions obtained while diagonalizing the energy operator matrix were used for calculations of the electron transition characteristics.

The obtained results were compared with data presented by other authors. The *ab initio* energy spectra of six investigated configurations are presented as a graph in Figure 3.2. In Figure 3.3 the experimental energy levels from [29] are plotted. As it is seen from these figures the theoretical *ab initio* results cover much larger area of the energy spectra than it is investigated experimentally. The detailed comparison of the obtained *ab initio* results with the experimental ones seems to be a rather complicated task due to extreme mixing of configurations. It is seen when analysing the results that neither usual LS-coupling scheme, nor jj-coupling often used for heavy ions is suitable for description of the levels of W II. One can see from the percentage composition that majority of levels are made of levels of different configurations of a same parity. The level $44354_{5/2}$ can be an example. The level is composed of 22% $5d^4(^5D)6p\ ^6D$ and

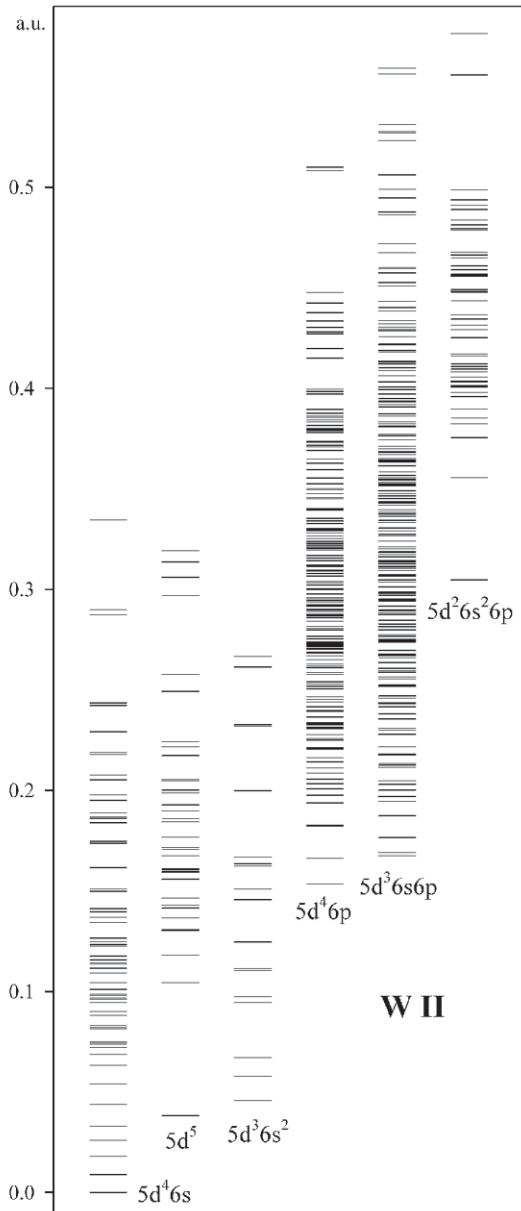


Figure 3.2
Theoretical energy spectra W II

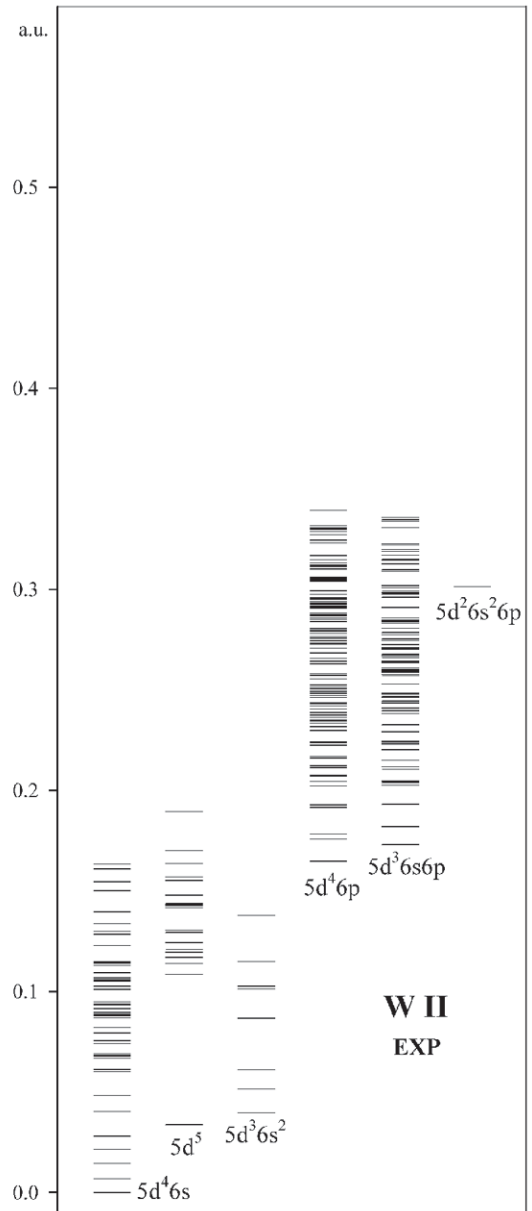


Figure 3.3
Experimental energy spectra W II

13% $5d^3(^4F)6s6p\ ^6D$ + 9% $5d^3(b^4F)6s6p\ ^4D$ [29], and from the QR results this level is 27% $5d^4(^5D)6p^6D$ and 16% $5d^3(^4F)6s6p\ ^6D$ + 6% $5d^3(^4F)6s6p^4D$. This example is typical for W II ion where only some levels are composed of components with one major contribution above 50%. Thus only limited number of levels can be attributed to the specific configuration.

Though the mixing is rather strong and the number of theoretical energy levels significantly exceeds the amount of experimental data it is still possible to select necessary theoretical data and link them to experimentally identified levels. Using the experimental energy values, calculated percentage composition and Lande factors from [29] and analogous QR results a Table 3.6 is developed. In the table the notation of the levels with the value of the total momentum

is presented. The energy value obtained within the quasirelativistic approach (E_{QR}) and lifetimes of the levels – experimental $\bar{\tau}_{exp}$ [30] and quasirelativistic $\bar{\tau}_{QR}$ ones, are presented there as well.

Table 3.6 Lifetimes of the excited levels of W II

<i>Level</i>	$E_{QR} (cm^{-1})$	$\tau_{EXP} (ns)$	$\tau_{QR} (ns)$
36165 _{1/2}	33700	14.42	12.40
38576 _{1/2}	36466	11.88	11.40
39129 _{3/2}	37127	13.94	17.60
42049 _{5/2}	40061	11.07	9.01
42298 _{3/2}	40002	10.88	13.10
42390 _{7/2}	41106	76.1	67.10
44354 _{5/2}	42499	9.90	16.30
44455 _{1/2}	42724	2.67	7.05
44758 _{9/2}	43181	21.63	14.70
44877 _{7/2}	42600	6.58	8.03
44911 _{3/2}	43291	4.35	7.39
45553 _{3/2}	44070	7.88	5.80
46493 _{9/2}	44573	12.37	20.90
47179 _{3/2}	44938	5.8	6.41
47588 _{3/2}	45124	3.40	3.05
48284 _{5/2}	46819	5.9	3.40
48982 _{3/2}	46428	5.00	5.50
49181 _{9/2}	47044	21.5	19.60
49242 _{5/2}	45777	3.33	5.85
50292 _{5/2}	47872	5.14	6.71
50430 _{3/2}	48399	6.6	6.02
51045 _{7/2}	48661	4.7	4.52
51254 _{3/2}	49986	2.1	1.76
51438 _{5/2}	49394	4.6	5.69
51495 _{11/2}	48553	7.7	9.36
54229 _{11/2}	52644	2.48	2.37
54498 _{7/2}	53555	2.1	2.87
55392 _{9/2}	53992	2.3	2.58

The theoretical lifetimes are calculated taking into account not only the probabilities of the one-electron dipole transitions but also two-electron transitions. The values of the experimental and quasirelativistic lifetimes are rather close. The differences make only from few to few tens percents, except the level 44455_{1/2}, which experimental lifetime is 2.5 times smaller than the one obtained by the quasirelativistic approach. As it is seen from the Table 3.6 the *ab initio* energy levels obtained within the quasirelativistic approach deviate from the experimental ones by 2000 cm⁻¹ on average that makes 4%. The differences are larger for lower energy levels and smaller for more excited levels in cases of other levels from [29] which we managed to compare with QR results.

As already mentioned, *ab initio* quasirelativistic energy spectra obtained cover much wider energy area than the experimental results. Thus new data on the possible transitions from the highly excited levels of configurations 5d⁴6p, 5d³6s6p and 5d²6s²6p are obtained. In order to

evaluate the accuracy of the obtained quasirelativistic wavelengths, they were compared to the experimental ones from [30]. The results of the comparison revealed that wavelengths obtained by the quasirelativistic approach are 4-7% longer than the experimental ones. In Table 3.7 the emission transitions with highest theoretical probabilities are presented. Their initial levels are not experimentally identified. The identification of the levels in this table is rather formal made according to the theoretical mixing of levels.

Table 3.7. Characteristics of most probable transition of W II obtained within quasirelativistic approach

<i>Upper level</i>	<i>Lower level</i>	$\lambda(\text{\AA})$	<i>gf</i>	<i>A (s⁻¹)</i>
5d ³ (² H)6s6p ² G _{9/2}	5d ³ 6s ² ² H _{11/2}	1557	6.96×10 ⁰	1.91×10 ⁹
5d ³ (² D)6s6p ² P _{3/2}	5d ³ 6s ² ² D _{5/2}	1545	1.63×10 ⁰	1.14×10 ⁹
5d ³ (² D)6s6p ² P _{1/2}	5d ³ 6s ² ² D _{3/2}	1557	7.35×10 ⁻¹	1.01×10 ⁹
5d ³ (² H)6s6p ² I _{13/2}	5d ³ 6s ² ² H _{11/2}	1847	6.45×10 ⁰	9.00×10 ⁸
5d ³ (² D)6s6p ² P _{1/2}	5d ⁴ (¹ D)6s ² D _{3/2}	1676	7.34×10 ⁻¹	8.71×10 ⁸
5d ² (³ P)6s ² 6p ² D _{3/2}	5d ³ 6s ² ² F _{5/2}	1739	1.46×10 ⁰	8.03×10 ⁸
5d ³ (² D)6s6p ² P _{1/2}	5d ³ 6s ² ² D _{3/2}	1488	4.64×10 ⁻¹	6.99×10 ⁸
5d ³ (² H)6s6p ⁴ H _{13/2}	5d ⁴ (³ H)6s ⁴ H _{13/2}	2069	5.86×10 ⁰	6.52×10 ⁸
5d ³ (² D)6s6p ² P _{3/2}	5d ⁴ (¹ D)6s ² D _{5/2}	1709	1.06×10 ⁰	6.03×10 ⁸
5d ³ (⁴ F)6s6p ⁴ D _{1/2}	5d ³ (⁴ F)6s ² _{3/2}	1562	4.24×10 ⁻¹	5.80×10 ⁸
5d ³ (² D)6s6p ² D _{3/2}	5d ³ 6s ² ² D _{3/2}	1775	1.07×10 ⁰	5.69×10 ⁸
5d ³ (⁴ P)6s6p ⁴ D _{7/2}	5d ³ 6s ² ⁴ F _{9/2}	1482	1.45×10 ⁰	5.51×10 ⁸
5d ³ (² D)6s6p ² F _{5/2}	5d ³ 6s ² ² D _{5/2}	1690	1.40×10 ⁰	5.45×10 ⁸
5d ² (³ P)6s ² 6p ² S _{1/2}	5d ³ 6s ² ² P _{1/2}	1446	3.37×10 ⁻¹	5.37×10 ⁸
5d ³ (² D)6s6p ² F _{7/2}	5d ³ 6s ² ² D _{5/2}	1716	1.89×10 ⁰	5.36×10 ⁸
5d ³ (² D)6s6p ² D _{5/2}	5d ³ 6s ² ² F _{7/2}	1545	1.12×10 ⁰	5.20×10 ⁸
5d ² (¹ G)6s ² ² G _{7/2}	5d ⁴ (³ H)6s ² H _{9/2}	1470	1.33×10 ⁰	5.13×10 ⁸
5d ³ (⁴ F)6s6p ⁴ F _{3/2}	5d ⁴ (³ F)6s ⁴ F _{3/2}	1773	9.50×10 ⁻¹	5.04×10 ⁸
5d ³ (² H)6s6p ² H _{9/2}	5d ³ 6s ² ⁴ F _{9/2}	1659	2.08×10 ⁰	5.04×10 ⁸
5d ³ (² D)6s6p ² D _{3/2}	5d ³ 6s ² ² F _{5/2}	1563	7.34×10 ⁻¹	5.00×10 ⁸

Analyzing the *ab initio* results and comparing them to the experimental ones one can see, that preliminary results, although not very accurate, of the theoretical investigation are rather reliable and allow to evaluate the effectiveness of the methods in use and foresee the methods to improve them. In order to obtain more precise energy spectra it is planned to enlarge the basis of the quasirelativistic radial orbitals and to increase the number of the admixed configurations including the configurations with an open 5p-shell into the superposition thus taking into account the correlation effects caused by polarisation of 5p-shell. It is planned to evaluate the influence of electric quadruple and magnetic dipole transitions on theoretically calculated lifetimes of the excited energy levels. Described results of the investigation of W II were presented at the international conference [31] and prepared for publication [32].

3.4 Investigation of Auger cascades and relaxation effects following the production of a vacancy by electron impact in the tungsten W^+ , W^{3+} and W^{5+} ions

The multiple ionization of tungsten ions during their collisions with electrons can influence the distribution of such ions in the tokamak plasma [33]. The double and triple ionization of tungsten ions by electron impact at low ionization stages was measured and described by the semi-empirical formula in [34], but no ab initio calculations were made. Theoretical treatment enables to perform the detailed analysis, to reveal the contributions from various elementary processes and shells. Earlier we performed the calculation of double ionization for neutral tungsten atoms and W^{2+} , W^{4+} and W^{6+} ions [35]. The aim of the present work was to investigate the Auger cascades and relaxation effects following the production of a vacancy by electron impact in the tungsten W^+ , W^{3+} and W^{5+} ions, and to use these results for the calculation of double and triple ionization cross sections.

Calculations of energy level spectra, Auger transitions rates as well as cross sections of single ionization and excitation by electron impact have been performed in the relativistic approximation using Flexible Atomic Code [36]. According to [37] this code is highly suitable for multiple charged ions of heavy elements. The mixing of all relativistic configurations corresponding to the same nonrelativistic configuration was taken into account. The probabilities of direct multielectron ionization in sudden perturbation model have been calculated with original program using the quasirelativistic wave functions [22].

The deexcitation of states with an initial inner vacancy at low ionization stages is performed mainly by nonradiative Auger transitions. At energies of electron beam till 1000 eV used in the experiment [34] the electrons can be removed from shells of ions with the principle quantum number $n=4$ and $n=5$. However, in this interval of energies the single ionization cross sections for 4s, 4p, 4d and 5s shells obtains considerably smaller values than for the 5p and 4f shells, thus practically only cascades during the deexcitation of states with vacancies in these shells give the main contribution to the production of higher ions. While Auger transitions take place between the neighboring or overlapping configurations the detailed level-by-level calculations must be performed. According to the diagram of energy level spectra (Figure 3.4) the most of the cascades end in the following stage of ionization, thus the role of Auger cascade in the triple ionization process is obtained rather small.

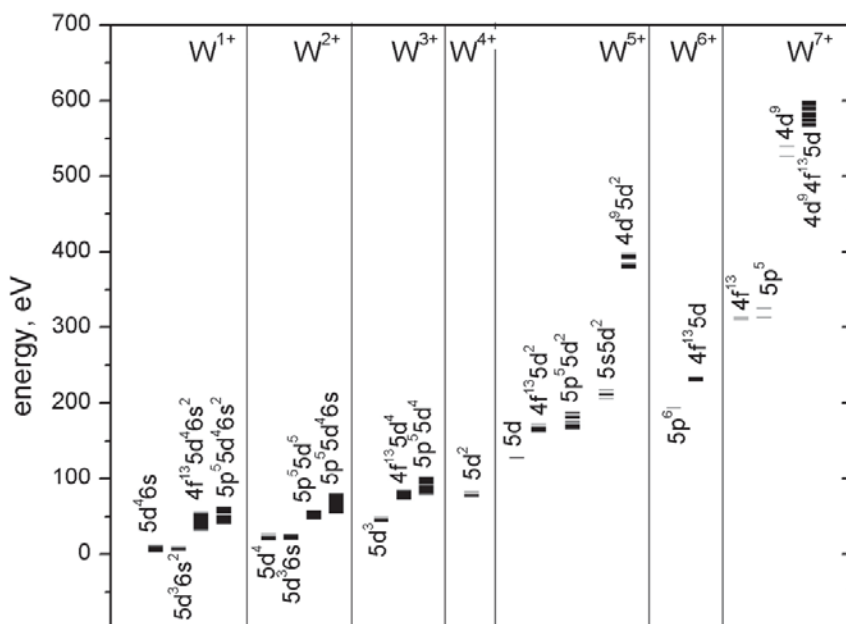


Figure 3.4
Energy level spectra of ions involved in Auger transitions after ionization of initial ion

The direct multiple ionization by electron impact can be approximately described in the sudden perturbation approximation as a two step process: production of an inner vacancy and subsequent additional ionization of ion due to relaxation of electronic shells (shake effect). The probability of the last process is expressed as a product of probabilities to remove one or more electrons and probability to stay the other electrons in their shells. The corresponding formulae can be obtained by simple statistical consideration [38]. For example, the probability that after the single ionization of $n_0 l_0^{N_0}$ shell two electrons will be removed from the same $n l^N$ shell obtains the expression:

$$A(n_0 l_0^{-1} n l^{-2}) = \frac{N(N-1)}{2} \left[1 - \langle n l_K | n l_{K_1} \rangle^2 \right] \left[1 - \langle n l_K | n l_{K_1} \rangle^2 \right] \langle n l_K | n l_{K'} \rangle^{2(N-2)} \quad (10)$$

where $\langle n l_K | n l_{K'} \rangle$ is the overlap integral of radial orbitals, subscript indicates the configuration, which wave functions are used for the calculations of this integral: K is the initial configuration without vacancies and $K, a'' K n_0 l_0^{-1}$. Most of the states with a vacancy and an excited electron autoionizes into a state of the next ion [39], thus the expression (10) takes into account not only shake-off effect (transition of electron to the continuum state), but also shake-up effect (excitation of electron to the higher discrete state). Only energetically possible shake transitions must be included.

The larger value of shake probability is obtained at the production of vacancy in a deeper shell. In neutral atoms it reaches 0.18 for single and 0.015 for double ionization following the production of $4d^{-1}$ vacancy. The probability to remove one or two additional electrons diminishes on increasing the ionization degree, to a larger extent in the case of two removed electrons (Figure 3.5).

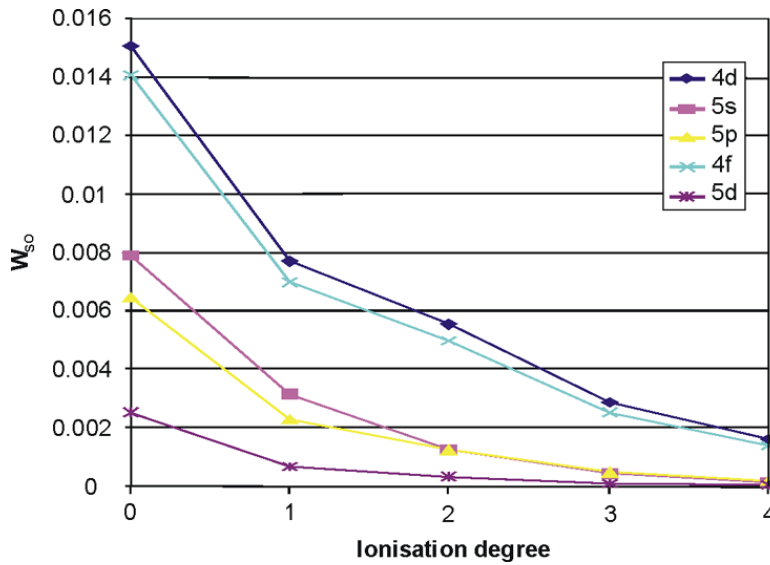


Figure 3.5
The values of the probability to remove two electrons from any other shell due to sudden perturbation (W_{so}) at the production of indicated initial vacancy

The obtained probabilities of Auger transitions and shake effect have been used to calculate the cross sections of double and triple ionization of tungsten ions by electron impact. The necessary single ionization cross section for W^{3+} and W^{6+} was obtained in the relativistic distorted wave approximation, for W^{1+} in the more exact for such ion binary-encounter-dipole approximation [40]. Also the indirect ionization process of excitation-autoionization is included. It gives a significant contribution to single ionization cross section for such tungsten ions. The contributions from the Auger transitions and from the sudden perturbation to the double ionization cross section are of the same order, though the last process plays a smaller role, especially for the higher ions. The calculated cross section of double ionization for considered ions agree qualitatively with

the experimental data. However, the cross section of triple ionization is obtained essentially smaller than its measured values. The main reasons must be the correlation effects as well as the inaccuracy of sudden perturbation model at energies comparable with the binding energies of electrons.

Performed in the present work the large scale calculations of Auger cascades and of additional ionization due to relaxation effects reveal the contributions of both processes as well of various shells to the double ionization of tungsten ions by electron impact. Such analysis of less probable triple ionization requires performing more accurate calculations. Only then the estimation of possible influence of multiple ionization processes on the distribution of tungsten ions in the tokamak plasma will be possible.

The results of this work were reported at the Europhysics conference [41] and partially presented in the paper [35].

3.5 Relativistic electron-ion scattering calculation

One of the sources of energy losses in fusion plasma is a radiation from impurities. By solving the balance equations, it is possible to determine the level populations of different ionization stages and subsequently to determine energy losses and synthetic emission-line spectra originating from impurities. In order to construct balance equations for a wide range of ionization degrees, one need to know in detail accurate atomic parameters describing atomic (ionic) energy structure (energy levels, radiative transition probabilities, Auger transition rates) and photon or charged particle scattering from ionized atoms.

The scattering problem has to do with all different processes that can occur after a collision of an ion with a photon or with a charged particle. Both theoretical and experimental methods of obtaining scattering parameters are very complicated, especially when dealing with highly-charged high-Z ions. Hence we need to develop sophisticated theoretical methods and models allowing to simplify or to reduce calculations required for a large scale scattering data generation and data bases production.

Several theoretical methods suitable for electron scattering calculations are established and widely used in practical applications. One of the most accurate and suitable technique to accurately solve the scattering problem is the R-matrix method. The method includes nearly all of the physical effects that contribute to electron-ion scattering cross sections and is applicable to all kinds of atoms, from neutral to highly ionized stages. It is well suited to solve theoretically the problem of electron scattering on multi-charged tungsten ions since it is able to include relativistic effects.

Unfortunately, these calculations are prohibitively large and extremely time-consuming if performed in the relativistic coupling with the Dirac-Fock R-matrix method employed because the accuracy of results depends on the number of target levels included. This number is significantly larger comparing to a non-relativistic *LS*-term case. The methods based on transformation of *S*- and *K*- matrices, calculated in the pure *LS*-coupling, to intermediate coupling can help to overcome the problem because the number of terms is considerably smaller than number of corresponding levels making these terms. On the negative side, only the non-relativistic wave functions are used in the *LS*- coupling. This kind of approximation becomes unsuitable and unsustainable when one has to deal with the highly-charged heavy ions where it is extremely important to use the relativistic wave functions and the appropriate relativistic approximations.

We have developed an approach based on the analogues of the relativistic integrals (ARI). This method enables us to employ the best aspects of non-relativistic and completely relativistic approach; a relatively small *LS*-basis and accurate relativistic wave functions from Dirac-Fock approximation.

The main goal of the research is the assessment of different methods to implement the relativistic R-matrix approach in the calculation of atomic data for electron scattering from the highly-charged tungsten ions and the estimation of the importance of correlation and relativistic effects

in the case of the electron-impact excitation from the outer shells of heavy ions. As an initial step for the electron-ion scattering calculations, the extended basis of relativistic wave functions based on the Dirac-Fock type radial orbitals was obtained. Relativistic wave functions were determined for the ground state and for the excited states with outer electron in $4l, 5l', 6l'', 7l'''$ shells of the W^{45+} ions when $l = 0, 1, 2, 3; l' = 0, 1, 2, 3, 4; l'' = 0, 1, 2, 3, 4, 5; l''' = 0, 1, 2, 3, 4, 5, 6$. Different basis sets of interacting configurations (which determine the accuracy and the size of the calculations) were considered.

One of the ways to assess the accuracy of the computed wave functions is to compare calculated energy levels with other theoretical data and existing experimental results. In the first phase of the current project, we have compared the energies of the W^{45+} ion levels obtained in our calculations with the existing experimental data and with available theoretical calculations which employ a different approach. We have performed calculations with well-established and widely recognised relativistic atomic-structure package GRASP using the different numbers of configurations in the CI expansion of wave function. The lowest number of the included levels was 52 and it was gradually increased up to 93 levels. Similarly, we have performed calculations with another relativistic code FAC which employs a different type of radial orbitals. Using above described technique to evaluate the accuracy of our theoretical data, it was established that we have achieved a reliable agreement with the experimental. Thus we can assume that our data have the required accuracy and the CI wave function basis for the further calculation of electron-ion scattering process has been established.

In Table 3.8 we compare the energies of levels up to $n = 6$ of the W^{45+} ion from our calculation with experimental data and with available theoretical calculations (DARC).

Table 3.8. Energies of levels up to $n = 6$ of the W^{45+} ion

<i>Level</i>	<i>Experiment</i>	<i>DARC</i>	<i>Our calculation</i>		
			<i>FAC</i>	<i>GRASP93</i>	<i>GRASP52</i>
$4s_{1/2}$	0	0	0	0	0
$4p_{1/2}$	787.46	792.306	788.232	790.508	790.331
$4p_{3/2}$	1605.0	1616.606	1605.575	1613.949	1613.906
$4d_{3/2}$	2819.9	2837.584	2823.101	2835.575	2835.369
$4d_{5/2}$	2994.4	3014.694	2996.712	3012.520	3012.342
$4f_{5/2}$	4293.7	4315.894	4294.384	4313.302	4313.120
$4f_{7/2}$	4337.8	4361.944	4338.086	4359.169	4359.048
$5s_{1/2}$	7802.4	7813.857	7797.204	7808.293	7808.622
$5p_{1/2}$		8198.423	8179.873	8192.033	8192.313
$5p_{3/2}$	8573.4	8585.449	8563.096	8578.780	8579.092
$5d_{3/2}$	9145.2	9167.216	9142.871	9161.080	9161.338
$5d_{5/2}$	9233.4	9253.108	9226.858	9246.910	9247.174
$5f_{5/2}$	9809.4	9830.501	9803.552	9823.977	9824.264
$5f_{7/2}$	9834.3	9856.901	9828.910	9850.342	9850.588
$5g_{7/2}$	10129	10150.860	10116.627	10141.998	10142.57
$5g_{9/2}$	10140	10161.364	10126.879	10152.500	10153.080
$6f_{5/2}$	12796	12818.338	12805.235	12810.446	12810.898
$6f_{7/2}$	12817	12834.109	12821.098	12826.169	12826.627
$6g_{7/2}$	12982	1299.9310	12984.025	12990.030	12990.897
$6g_{9/2}$	12981	1300.5510	12990.199	12996.499	12997.096

3.6 Calculation of collision strengths for the W^{45+} ions using relativistic R-matrix code

For the purpose of electron-ion scattering calculations, the non-relativistic R-matrix code that uses the relativistic analogues of integrals was extended for the general case of complex configurations, enabling its application for the configurations and the ions under consideration.

The target orbitals were generated with the AUTOSTRUCTURE code [43, 44] (<http://amdpp.phys.strath.ac.uk/autos/>) for the nonrelativistic calculations.

The relativistic R-matrix calculations employing regular scattering codes from the DARC suite of codes were performed for the electrons of $n = 4$ shell. These data can serve as a benchmark point for the comparison with the data, obtained from the non-relativistic R-matrix method based on the multichannel quantum defect theory and intermediate coupling frame transformation with the non-relativistic interaction integrals replaced by their relativistic versions.

The comparison of electron-impact excitation calculation results obtained using three different methods is presented in Figure 3.6, Figure 3.7, Figure 3.8.

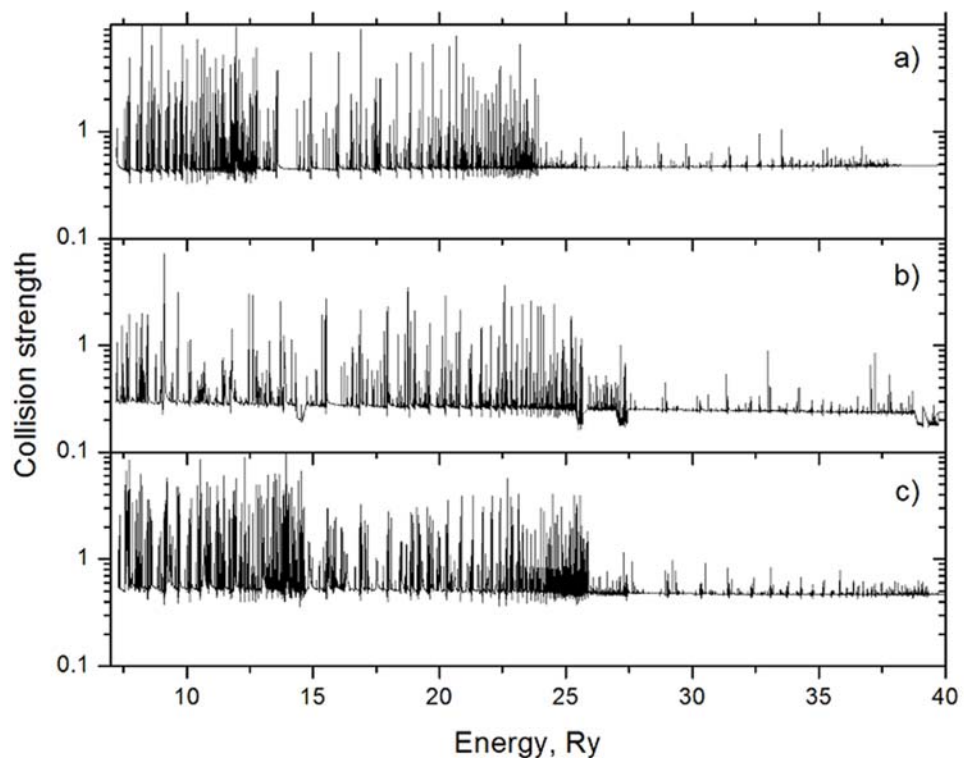


Figure 3.6 Electron impact excitation collision strengths for the $4s_{1/2} - 4p_{1/2}$ transition in W^{45+} . Data obtained with (a) the nonrelativistic R-matrix code (ICFT), (b) the relativistic R-matrix code (DARC-OXQUB) and (c) the nonrelativistic R-matrix code that uses the relativistic analogues of integrals

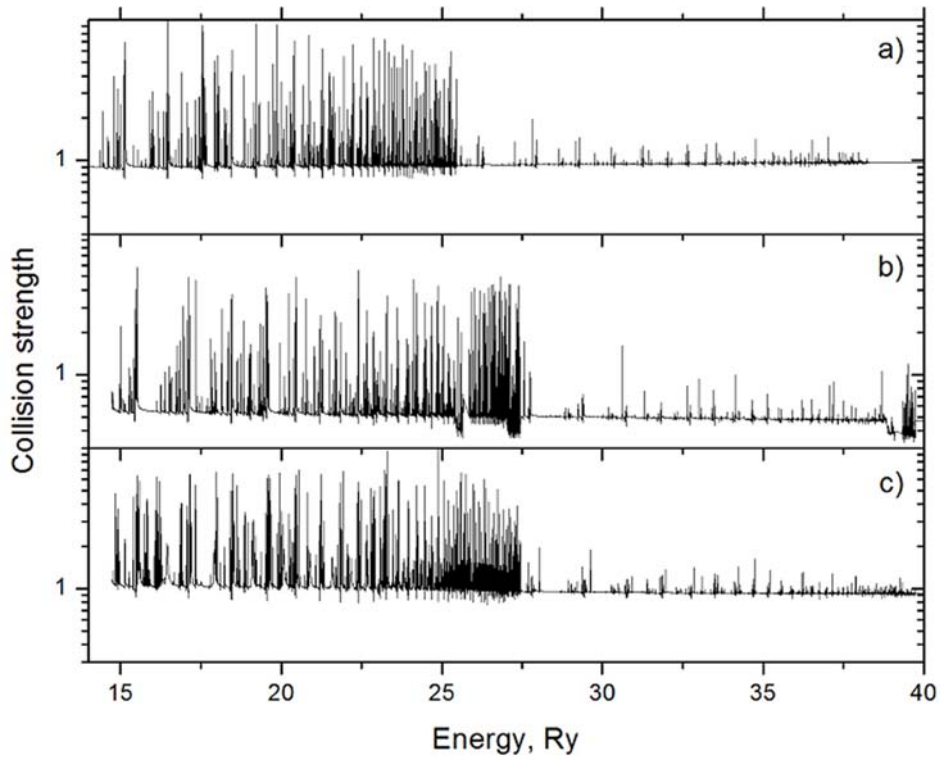


Figure 3.7
 Electron impact excitation collision strengths for the $4s_{1/2} - 4p_{3/2}$ transition in W^{45+} . Data obtained with (a) the nonrelativistic R-matrix code (ICFT), (b) the relativistic R-matrix code (DARC-OXQUB) and (c) the nonrelativistic R-matrix code that uses the relativistic analogues of integrals

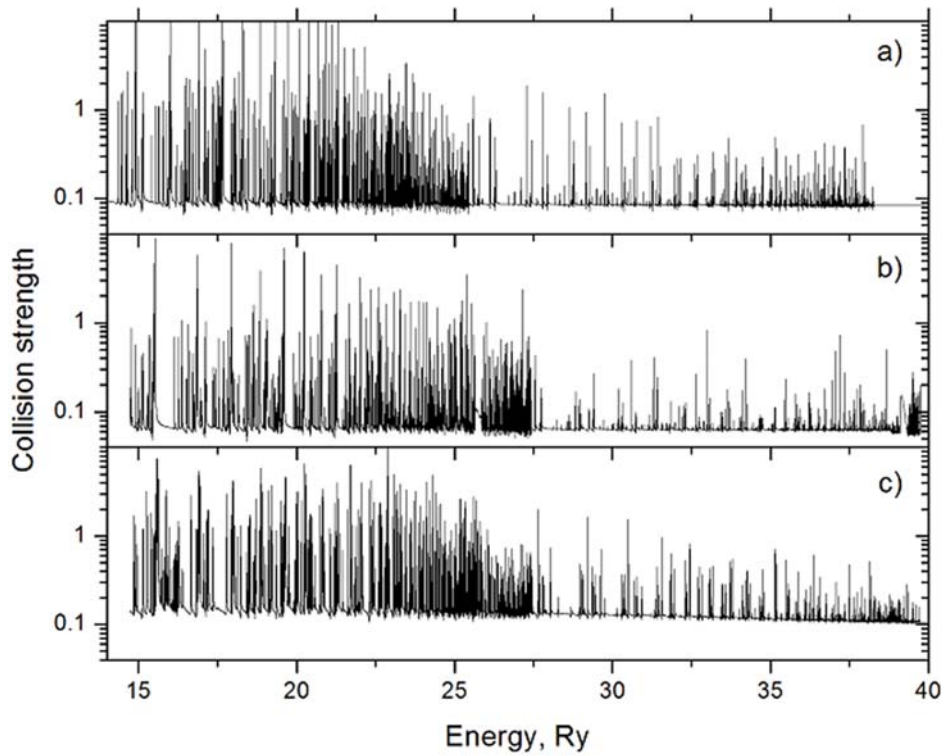


Figure 3.8
 Electron impact excitation collision strengths for the $4p_{1/2} - 4p_{3/2}$ transition in W^{45+} . Data obtained with (a) the nonrelativistic R-matrix code (ICFT), (b) the relativistic R-matrix code (DARC-OXQUB) and (c) the nonrelativistic R-matrix code that uses the relativistic analogues of integrals

It can be seen that a resonance structure in cases where relativistic wavefunctions are used is very similar. Some non-essential differences are influenced by the deviations in energy levels structure and by the fact that the energy mesh is not fine enough. Therefore the resonances of collision strengths are not delineated precisely enough. Furthermore, backgrounds of collision strengths are lower compared with nonrelativistic results. However collision strengths obtained with relativistic analogues of integrals are higher than calculated in fully relativistic approximations.

Based on the results presented here and from our wider studies on the project, we can conclude that for highly charged and heavy elements the relativistic wave functions have to be employed in calculations. Approach where nonrelativistic integrals are substituted by their relativistic analogues extends applications of ready-available computer codes. Fairly good agreement with Dirac-Fock values is obtained for energy levels of $4l$ ($l=0,1,2,3$) configurations for W^{45+} ion where calculations performed with relativistic analogues of integrals.

The comparison of electron-impact excitation collision strengths obtained with relativistic and non-relativistic wavefunctions for the transitions in the W^{45+} ions demonstrates reasonable agreement of produced data for the highly charged tungsten ion. However, the non-relativistic calculations slightly overestimate collision strengths if compared with the approaches where relativistic wavefunctions were used.

3.7 Theoretical study of magnetic dipole transitions using Dirac-Fock approach

Many studies have been devoted to the interpretation of spectra from highly ionized tungsten ions recorded in EBIT experiment. EBIT construction allows trapping ions of the element which are mainly in the same ionization state. Therefore, assigning lines of observed spectra to the particular ions is much easier in comparison with radiation spectra from other sources. Additionally, the number of elementary processes that take place in the EBIT plasma is smaller as well and what allows one to model them with confidence.

Magnetic dipole transitions are often of particular interest due to their sensitivity to plasma parameters such as electron temperature and density. Recently magnetic dipole spectra corresponding to the transitions between levels of the ground $4d^N$ ($N=1, \dots, 9$) configurations of $W^{37+} - W^{29+}$ ions were observed by Berlin EBIT [45, 46]. However it was shown that the basis of six configurations used for the calculation of wavelengths was insufficient to identify the measured lines correctly. Furthermore, the collision radiative modelling using set of six even-parity configurations with additional two odd-parity $4d^{N-1}$ and $4p^5 4d^{N+1}$ configurations does not allow reproducing well line intensities of the experimental spectra especially for the tungsten ions having near half-filled 4d shell where configurations correspond to the large number of energy levels.

In contrast to the wavelengths and transition probabilities generated with atomic structure program FAC, here we use multiconfiguration Dirac-Fock method implemented in GRASP2K code [47, 48]. Therefore the aim of this work is to report energy levels, wavelengths and transition probabilities for magnetic dipole transitions among the levels $4d^N$ ($N=1, \dots, 9$) configurations in multiconfiguration Dirac-Fock approach using extended configuration interaction (CI) basis.

The CI strength:

$$T(K, K') = \frac{\sum_{\gamma \gamma'} \langle K \gamma | H | K' \gamma' \rangle^2}{\bar{E}(K, K')^2} \quad (11)$$

introduced previously in [22, 49, 50] has been employed to find a set of the most strongly interacting configurations with the $4d^N$ configurations in tungsten ions. The quantity in the

numerator of Eq. (11) is the interconfiguration matrix element of the Hamiltonian H and $\bar{E}(K, K')^2$ is the energy distance between the interacting levels of configurations K and K' :

$$\bar{E}(K, K') = \frac{\sum_{\gamma\gamma'} [\langle K\gamma | H | K\gamma \rangle - \langle K'\gamma' | H | K'\gamma' \rangle] \langle K\gamma | H | K'\gamma' \rangle^2}{\sum_{\gamma\gamma'} \langle K\gamma | H | K'\gamma' \rangle^2} \quad (12)$$

The summation in (11) and (12) is performed over all states γ and γ' of both configurations.

Calculation of the CI strength for the several hundreds of configurations is performed by using the method of global characteristics [49, 50]. The method allows to express the summation over configuration states by the summation over one- and two-electron integrals with simple factors. Due to this the CI strength for large number of configurations differing by one or two electrons from the considered configuration can be easily estimated using personal computers. The same approach has successfully been applied for theoretical investigation of transitions in tungsten, transition metals and even the cascade of Auger processes.

The one- and two-electron excitations from the $n=3$ complex have been included to obtain the set of configurations for which CI strengths with $4d^N$ configuration have been calculated. The one-electron excitations are taken up to the shells of $n=7$ complex while the two-electron excitations include only shells up to $n=5$ complex.

Previous results obtained by Dirac-Fock-Slater calculations are compared with our data for the ground level energies of the $4d^N$ ($N=1, \dots, 9$) configurations in Table 3.9. It can be seen that the multiconfiguration Dirac-Fock energies are lower than ones obtained earlier by about 14 a.u. The main reason of the difference is that FAC uses the local approximation of the exchange interaction to generate one-electron orbitals. It can be stated that the exchange effects are underestimated when solving coupled Dirac equations in Dirac-Fock-Slater method adopted by FAC. The most interesting fact is that the difference does not vary significantly for the different ionization states.

Table 3.9. The ground and highest state energies for the $4d^N$ ($N=1, \dots, 9$) configurations obtained in Dirac-Fock-Slater and Dirac-Fock approximations.

<i>Ion</i>	<i>Ground state</i>		<i>Highest state</i>	
	<i>DFS</i>	<i>DF</i>	<i>DFS</i>	<i>DF</i>
W ²⁹⁺	-15722.6	-15737.4	0.606	0.602
W ³⁰⁺	-15679.5	-15694.2	1.605	1.598
W ³¹⁺	-15634.4	-15649.1	2.034	2.03
W ³²⁺	-15587.3	-15602.1	2.702	2.698
W ³³⁺	-15538.4	-15553.1	2.742	15553
W ³⁴⁺	-15487.6	-15502.3	3.233	3.228
W ³⁵⁺	-15434.2	-15448.9	2.324	2.319
W ³⁶⁺	-15378.8	-15393.3	1.843	1.845
W ³⁷⁺	-15321.1	-15335.9	0.705	0.701

Since all energies of the ground states calculated by FAC are larger by the similar amount in comparison with GRASP2K calculations, the ionization energies in both cases are similar too. It

should be noted that the different number of configurations were used to generate both data. Much larger CI basis is employed here using fully relativistic approach. Number of configurations used in GRASP2K calculations varies from ion to ion: W^{29+} - 129 configurations, W^{30+} - 91, W^{31+} - 61, W^{32+} - 60, W^{33+} - 41, W^{34+} - 71, W^{35+} - 63, W^{36+} - 87, W^{37+} - 202. The CI strength calculated in every case to take into account the admixed configurations in a systematic way.

As well Table 3.9 comprises calculated energies of the highest levels for $4d^N$ ($N=1, \dots, 9$) configurations with respect to the ground state. The results confirm the fact that the splitting of levels is similar in both sets of data.

The calculations demonstrate the importance of *jj*-coupling scheme for the configurations of heavy elements like highly charged states of tungsten. Leading percentage compositions for intermediate wavefunctions exceed 70 % for many levels.

The comparison of wavelengths and radiative rates obtained by Dirac-Fock-Slater and Dirac-Fock approximations is presented in Table 3.10. The difference of the analogous wavelengths obtained by Dirac-Fock-Slater calculations is generally smaller than 0.4 %. Practically all wavelengths calculated in Dirac-Fock approximation are larger when compared with the values obtained using Dirac-Fock-Slater method. Only six transitions in Table 3.10 have smaller wavelengths in comparison with previous results obtained by FAC. These discrepancies can be related to the different approaches employed in calculations of radial orbitals. Additionally, the larger CI bases employed in GRASP2K calculations diminish the energetic distances between levels.

The values from experimental measurements where HULLAC calculations with CI basis of six configurations were applied for the line interpretation are shown in Table 3.10 as well. However the identification of lines based on HULLAC calculations for some wavelengths differs significantly from FAC and GRASP2K values. Therefore it confirms the suggestion that those lines with the largest discrepancies for wavelengths are wrongly identified.

By contrast to wavelengths, much larger discrepancies are obtained for GRASP2K radiative probabilities of the magnetic dipole transitions in comparison with FAC data. The negative and positive differences are observed. In the nonrelativistic limit, matrix element of the magnetic dipole operator does not involve radial integrals and contains summation over expansion coefficients of the wavefunction. Therefore the differences for transition probabilities take place because of different sets of the expansion coefficients obtained in those calculations.

By this we can conclude that the larger CI basis and the Dirac-Fock method employed in the current calculations have a crucial influence on the probabilities of the magnetic dipole transitions while the values of wavelengths change only by about 2 Å in comparison with FAC values.

3.8 Properties of Auger electrons following excitation of polarized atoms by polarized electrons

The general expression for the cross section describing the Auger decay following the excitation of polarized atoms by polarized electrons was obtained for the first time in such collisions in which the two-step approximation can be applied [50]. The expression describes the polarization states and angular distributions of all particles in both the initial and final states. The cross sections for some special cases, i.e. the angular distribution of the Auger electrons following excitation of non-polarized atoms by non-polarized electrons, the angular correlations between the Auger and scattered electrons following excitation of non-polarized atoms by non-polarized electrons, and the magnetic dichroism in the angular distribution of the Auger electrons following excitation of polarized atoms by non-polarized electrons are derived to demonstrate the applications of the general expression for specific experimental conditions.

Table 3.10. Comparison of some calculated wavelengths (λ) from FAC and GRASP2K codes with experimental values [36] assigned to the transitions among the levels of $4d^N$ ($N=1,\dots,9$) configurations. Radiative probabilities (A) for M1-type transitions are presented too.

	λ			A	
	<i>Exp[36]</i>	<i>FAC</i>	<i>GRASP2K</i>	<i>FAC</i>	<i>GRASP2K</i>
W ²⁹⁺	756.64	755.05	756.32	3.72E+04	2.48E+04
W ³⁰⁺	687.57	709.14	711.75	2.51E+04	1.51E+04
	790.31	783.21	784.10	2.81E+04	2.82E+04
	650.92	671.44	672.46	6.49E+04	4.65E+04
	794.21	788.74	788.99	4.68E+04	3.66E+04
	570.41	573.04	575.03	1.69E+04	1.69E+04
W ³¹⁺	804.88	800.22	800.37	4.97E+04	4.00E+04
	666.76	664.70	665.80	3.49E+04	3.53E+04
W ³²⁺	803.03	804.44	805.32	4.07E+04	4.12E+04
	668.19	670.18	670.92	2.18E+04	2.19E+04
W ³³⁺	661.08	664.58	666.13	9.20E+03	1.13E+04
	708.22	714.38	714.73	9.03E+04	9.10E+04
	706.18	705.73	707.03	2.12E+04	2.82E+04
W ³⁴⁺	692.36	691.46	692.10	5.57E+04	3.71E+04
	864.51	875.98	875.89	3.70E+04	3.74E+04
	855.63	863.67	864.67	4.08E+04	1.23E+05
	736.64	737.38	738.92	2.29E+04	2.81E+04
	696.95	697.96	699.25	4.97E+04	2.99E+04
W ³⁵⁺	680.60	690.57	691.08	1.23E+05	4.11E+04
	662.40	657.83	659.61	6.45E+04	1.08E+05
	566.54	564.86	565.64	3.90E+04	2.60E+04
	563.82	570.60	572.58	3.62E+04	5.45E+04
	615.34	616.83	619.05	2.19E+04	2.62E+04
	629.85	632.53	632.81	6.67E+04	6.70E+04
	622.30	638.17	640.46	1.39E+04	6.94E+03
	660.03	659.21	660.47	6.66E+04	6.69E+04
	659.20	660.95	662.73	7.27E+04	9.71E+04
	710.46	711.62	712.87	3.70E+04	3.70E+04
W ³⁶⁺	756.64	749.84	750.65	1.95E+04	2.44E+04
	774.76	772.96	772.19	3.15E+04	3.17E+04
	822.68	828.71	828.53	4.49E+04	6.76E+04
	526.19	531.50	531.97	1.27E+04	9.04E+03
	541.20	551.19	550.81	3.76E+03	2.27E+03
	574.30	584.02	584.14	2.76E+04	2.77E+04
	598.01	596.46	597.35	5.92E+04	7.63E+04
	635.89	635.08	635.55	4.77E+04	4.79E+04
	680.60	679.06	680.33	2.03E+04	3.39E+04
	707.74	711.52	711.45	5.35E+04	7.53E+04
W ³⁷⁺	795.09	797.77	797.27	1.55E+04	1.55E+04
	855.85	857.98	858.84	2.10E+04	6.32E+04
	646.68	647.35	649.61	3.97E+04	5.87E+04

3.9 Collaboration of VU ITPA with ADAS and JET

The contacts established in 2008 with Prof. H. Summers who is the leader of the ADAS (Atomic Data Analysis System) in JET were continued in 2009. Dr. V. Jonauskas has calculated ion yield data after processes of Auger cascade in tungsten ions W^{2+} , W^{4+} , W^{6+} and discussed the possibilities to use these data for the JET plasma diagnostics. It was decided that shake-off processes can be important for the double ionization rates in Auger cascade calculations and plasma diagnostics.

Dr. R. Kisielius carried out the installation, porting and testing of the Flexible Atomic Code (FAC) program package on a JET computer cluster in 2008. In 2009, this code was used for the calculations of the energy levels, Auger transition rates and dielectronic recombination rates for the autoionizing states of W^{13+} , W^{14+} , W^{7+} , and W^{8+} . The results were discussed with ADAS group members.

On October 4-7, 2009, Z. Rudzikas and R. Kisielius participated at the ADAS workshop held in Ringberg, Germany. At the workshop they presented the following reports:

1. R. Kisielius. Modified relativistic approach for atomic data calculation.
2. Z. Rudzikas. Complex many-electron highly charged ions investigations at ITPA.

On October 8-16, 2009, R. Kisielius participated at the ADAS-EU Course "ADAS, atomic calculations and their application to fusion plasma", which was held at Max-Planck-Institut für Plasmaphysik located in Garching, Munich.

4 MOBILITY PROGRAM 2009

During 2009 the following visits were implemented under the mobility plan:

3.4 Theory and modelling

It was planned to participate in one mission to UKAEA/Fusion, Culham, UK. The total duration of planned mission was 12 days. Due to changed plans this mission was cancelled.

4.7 Fusion safety issues

It was planned to participate in one mission to IPP-Griefswald, Germany. The total duration of planned mission was 24 days. This mission was implemented by visit of Tadas Kaliatka, Mantas Povilaitis, and Gintautas Dundulis to IPP-Griefswald on November 29 – December 5, 2009. The total duration of the visit 21 day.

A visit to facility W7-X was performed to see the current status of the W7-X facility.

LEI representatives
visiting W7-X at IPP



The final results on Leak-Before-Break analysis have been presented during the meeting with the KiP-group. It was shown that stress corrosion cracking growth as well as fatigue crack growth affected by the magnetic field will not reach critical values during the W7-X operation time. In fact, the probability of prompt double-ended rupture is very low, since a long time before small cracks and leaks will occur. It was concluded that further LBB analysis for W7-X is not necessary, but the experience of ITER with respect to LBB analysis will be used

Together with Mr. Naujoks the co-operation activities in 2009 and 2010 were discussed. It was agreed that LEI work in structural integrity area will be mainly related with strength analysis of port welds of W7-X facility.

The technical meeting with the expert of structural analysis department Mr. A. Tereshchenko was arranged. G. Dundulis presented 3D models of the ports AEU30, AEQ20 and AEK20. He explained the problems which arose in preparation of the models. Since the modelling of the port welds between the plasma vessel and the ports in the W7-X cryostat system is very time consuming and cannot be covered by the ongoing collaboration with respect to fusion safety

(topic 4.7 collaboration plan), it was decided to prepare a separate contract between IPP and LEI for limit analysis of the port welds between the plasma vessel and the ports. It was decided that a contract will be prepared when LEI will provide a FE model of the port AEU30 according to the IPP requirements.

Experimental facility W7-X was visited at IPP-Greifswald. Current status of the W7-X facility and various uncertainties due to missing data in the drawings was discussed.

Loss of coolant accident analysis was presented at the meeting with colleagues from IPP-Garching. Needs for additional design data were discussed. Device designers have participated and made comments on the performed analysis and obtained results.

Further co-operation activities possible in the year 2010 were discussed with Mr. Naujoks. It was agreed that LEI will perform more detailed analysis of the LOCA using new design data obtained from the IPP. IPP will provide the missing data, without which detailed simulations of the accident are not possible.

A visit to W7-X facility was performed to see the current status of the facility. The as-built facility was checked against the available drawings and schemas in order to clarify and update RELAP5 model of W7-X facility. In particular, the almost finished assembly work of the cooling circuits in the second basement has been shown together with their control systems. During this visit discussions were held with specialists who are responsible for the hydraulic part of W7-X facility. It was also useful to clarify and update RELAP5 model.

The thermal-hydraulic analysis of W7-X target cooling circuits in "baking" mode were presented at the meeting. There were presented results of analysis of double-ended break of DN40 pipe in the upper and lower targets, water hammer effect in the case of fast closure of automatic valves and others. At this meeting the colleagues from IPP-Garching have participated. They made comments and discussed on the performed analysis and received results.

Together with Mr. Naujoks the co-operation activities in 2009 and 2010 were discussed. It was agreed that RELAP5 model of W7-X facility will be updated according to the new received information and IPP will provide the data, which is still missing. Water hammer effect in the case of fast closure of automatic valves must be analysed in more details. It was decided to analyse very small water leak to plasma vessel.

Together with specialists of hydraulic part of W7-X facility was discussed technical details, which are important to perform planned work according to EURATOM/LEI association work schedule for 2009 and 2010.

Meetings under EFDA:

Egidijus Urbonavičius participated in Information Session on the New Mobility Agreement, which was held in Brussels on October 19, 2009. This meeting was not originally included in the mobility plan. The invitation to this meeting was received on July 31, 2009. The total duration of the visit 4 days instead of planned 3 days due to late arrival of the aircraft from Brussels to Prague airport.

At the meeting the presentations on the new mobility legal, organisational and financial aspects were given by the representatives of the European Commission. The participants were involved in discussions on the implementation of the new mobility agreement. The information received at the meeting is valuable and will be used in our association EURATOM/LEI.

Task Force PWI Meetings

It was planned to participate in PWI meeting in 2009, but due to changed plans this participation was cancelled.

5 PUBLIC INFORMATION

The information related with FUSION energy perspectives, last achievements in ITER development and other Fusion research fields is continuously distributed among universities, R&D institutions, schools:

- 18th March 2009. "Career days" at Kaunas Technology University, Kaunas Lithuania. Distribution of information and discussions on FUSION to students.
- 28-29th May 2009. 6th Conference of young scientists on energy issues CYSENI 2009 (www.cyseni.com). Conference is with regional (Estonia, Latvia, Lithuania, Belarus, Italy) attention. In the conference "Fusion energy" topic was included (1 of 11). Two papers were presented at the conference.
- 25th September 2009. FP7 project "Researchers night 2009". Distribution of information and discussions on FUSION to students.
- Article "Renewable energy is more than brain" in science popularisation magazine "Science and Life", 2009 No. 4 p.5-7, 40-41 by Prof. Jonas Grigas. A chapter (p. 41) is devoted to the fusion energy.
- Occasionally school teachers (physics, chemistry ...) from various regions of Lithuania visits Institute. In addition they receive information and brochures on fusion. Information is spread via personal contacts as well.
- Through our partner Vytautas Magnus University, which is located in Kaunas, Lithuania, the information is spread to schools when university looks for students to physics studies.

Popular lectures by **Olga Rancova** "The energy will be produced like in stars":

1. Festival of Science "Spaceship-Earth", Kaunas Jesuit Gymnasium, 16/09/2009;
2. Lithuanian Museum of Energetics, 21/04/2009;
3. Akmenės Gymnasium and 4 secondary schools, 22/04/2009;
4. Vilnius Sofija Kovalevskaja Secondary school, 28/04/2009;
5. Upynos community (Šilalės district) 23/05/2009;
6. Estate Kurtuvėnai (Telšiai district) 23/05/2009;
7. Science Festival "Star Nights", Astronomical Observatory of the VU Institute of Theoretical Physics and Astronomy, 17/05/2009.

6 PUBLICATIONS

- 6.1. P. Bogdanovich and O. Rancova, Quasirelativistic approach for ab initio study of highly charged ions // *Physica Scripta*, v. 78 (2008) 045301 (9 pp).
- 6.2. O. Rancova, P. Bogdanovich and R. Karpuškienė, Quasirelativistic ab initio study of Gallium like Molybdenum and Tungsten // *J Phys, Conf ser.*, vol. 163 (2009) 012011.
- 6.3. O. Rancova, P. Bogdanovich and R. Karpuškienė, Application of new quasirelativistic approach for treatment of oxygen-like Iron and Nickel // 40th EGAS Conference, Graz, 2008, Abstracts, p. 43.
- 6.4. P. Bogdanovich, O. Rancova and R. Karpuškienė, Quasirelativistic ab initio study of gallium-like molybdenum and tungsten // 14th International Conference on the Physics of Highly Charged Ions, HCI2008, Tokyo, Japan, Book of Abstracts, p. A-a10.
- 6.5. V. Jonauskas, S. Kučas and R. Karazija, Electron-impact double ionization of tungsten atoms and ions at low ionization stages, *Lith. J. Phys.* 49, 415-420 (2009).
- 6.6. S. Kučas, R. Karazija, V. Jonauskas, and A. Momkauskaitė, Interaction of $4p54dN+1$ and $4p64dN-14f$ Configurations and Its Influence on the Photoexcitation and Emission Spectra in the Isoelectronic and Isonuclear Sequences, *J. Phys. B* 42, 205001 (2009).
- 6.7. A. Kupliauskienė, V. Tutlys. Properties of Auger electrons following excitation of polarized atoms by polarized electrons // *Nucl. Instr. Meth. Phys. Res. B*, **267**, 263 (2009).
- 6.8. T. Kačegavičius Development of fusion facility W7-X model for ASTEC code // 5th conference of young scientists on energy issues CYSENI 2008, Kaunas, Lithuania, 29 May, 2008. Kaunas: LEI, 2008. ISSN 1822-7554, p. 1-10.
- 6.9. M. Povilaitis Simulation of thermonuclear plasma interaction with the first wall material // Radiation interaction with material and its use in technologies 2008: international conference, Kaunas University of Technology, September 24-27, 2008. Kaunas: Technologija, 2008. ISSN 1822-508X, p. 119-122.

7 IMPLEMENTATION OF QA SYSTEM

The quality assurance system according to standard LST EN ISO 9001:1995 requirements in Lithuanian Energy Institute has been developed in 1999.

In 2001 the updating of quality assurance system of institute on the basis of requirements of standard LST EN ISO 9001:2001 was initiated. According to these requirements the quality package of quality assurance documents in LEI was developed.

On February 17, 2004 the quality system of institute is certified by the Lithuanian Standards Board under the Ministry of Environment of the Republic of Lithuania and the certificate of quality management system conformity to standard LST EN ISO 9001:2001 is received. On February 15, 2007 duration of certificate was extended for next three years.

On February 15, 2010 the quality system of institute was certified by the Lithuanian Standards Board under the Ministry of Environment of the Republic of Lithuania and the certificate of quality management system conformity to standard LST EN ISO 9001:2008 was received.

On 15 February 2010 the environmental management system of institute was certified by the Lithuanian Standards Board under the Ministry of Environment of the Republic of Lithuania and the certificate of environmental management system conformity to standard LST EN ISO 14001:2005 was received.

The safety analysis of FUSION facilities is included in the procedure "PA/17-02, Control of nuclear installation safety research process", which is prepared in accordance with LST EN ISO 9001:2001 standards and operating together with other LEI quality management system procedures.

8 REFERENCES

1. D. Naujoks, Initial and Boundary Conditions, 1-NBF-T0008.0, Max-Planck-Institut für Plasma Physik, 2006.
2. E. Urbonavičius, D. Naujoks, Minutes of Meeting between IPP and LEI, Max-Planck-Institut für Plasmaphysik, LEI-IPP Co-operation, 1-NBF-C0010.0, IPP Greifswald, September 3 – 14, 2007.
3. C.D. Fletche, et. al., 1992. RELAP5/MOD3 code manual user's guidelines. Idaho National Engineering Lab., NUREG/CR-5535.
4. W. Klein-Hessling et. al., COCOSYS V1.2 Program Reference Manual, GRS-P-3/2, Gesellschaft für Anlagen- und Reaktorsicherheit (GRS) mbH, 2000.
5. A. Kaliatka, T. Kaliatka, V. Ognerubov, T. Kačėgavičius, Development of model for thermo-hydraulic analysis of processes in W7-X target cooling circuits in "baking" mode, Report No. S/17-887.7.8-01-V:01, Lithuanian Energy Institute, 2009.
6. A. Kaliatka, T. Kaliatka, V. Ognerubov, T. Kačėgavičius, Thermo-hydraulic analysis of DN40 mm pipe rupture in W7-X target supply line in "baking" mode. Results of RELAP5 modelling, Report No. S/17-887.7.8-03-V:02, Lithuanian Energy Institute, 2009.
7. G. Dundulis, R. Janulionis, R. Karalevičius, Leak before break analysis of W7-X target module, Report No. S/17-887.7.8-02-V:01, Lithuanian Energy Institute, 2009.
8. <http://www.solidworks.com>
9. R/H/R6 Document, 1996. Assessment of the Integrity of Structures Containing Defects. Nuclear Electric, R/H/R6 – Revision 3. – Gloucester: Nuclear Electric Ltd.
10. A procedure for safety assessment of components with cracks. Handbook, 3rd revised edition. P. Andersson, M. Bergman, B. Brickstad, L. Dahlberg, F. Nilsson, I. Satari-Far – Stockholm: SAQ Kontroll AB, 1996.
11. EUROPEAN COMMISSION NUCLEAR SAFETY AND THE ENVIRONMENT. European safety Practices on the Application of Leak Before Break Concept, Final report, EUR 18549 EN. (2000).
12. UNITED STATES NUCLEAR REGULATORY COMMISSION, US NRC Standard Review Plan, 3.6.3 Leak Before Break Evaluation Procedures, US NRC, Washington, DC (1986).
13. INTERNATIONAL ATOMIC ENERGY AGENCY, Applicability of the Leak Before Break Concept, IAEA-TECDOC-710, Vienna (1993).
14. P. Bogdanovich and O. Rancova, Phys. Rev. A 74, 052501 (2006).
15. P. Bogdanovich and O. Rancova, Phys. Rev. A 76, 012507 (2007).
16. P. Bogdanovich, Z. Rudzikas, and Šadžiuvienė, Acta Phys. Hung. 51,109 (1981).
17. R. Gįspįr, Acta Phys. Hung. XX, 151 (1952).
18. R. Gįspįr, Lietuvos Fizikos Rinkiny 3(1-2), 41 (1963).
19. A. Jucys, I.I. Glembockis, and R. Gįspįr, Acta Phys. Hung. 23, 425 (1967).
20. P. Bogdanovich, A. Bernotas, and A. Rinkevičius, Lith. J. of Phys., 49 (3) 253 (2009).
21. P. Bogdanovich and O. Rancova, Phys. Scr. 78, 045301 (2008).
22. R. D. Cowan, The Theory of Atomic Structure and Spectra (Berkeley, CA: University of California Press, 1981).

23. V. Jonauskas, S. Kucas and R. Karazija, *J. Phys. B: At. Mol. Opt. Phys.* 40, 2179 (2007).
24. A.E. Kramida and T. Shirai, *At. Data and Nucl. Data Tables* 95, 305 (2009).
25. P. Bogdanovich, V. Jonauskas, R. Karpuškienė, O. Rancova. Theoretical investigation of x-ray radiation of 4-4 transitions in highly charged tungsten ions // *Nucl. Instr. and Meth. A.* 2009, doi:10.1016/j.nima.2009.10.163.
26. O. Rancova, P. Bogdanovich, R. Karpuškienė, *J. Phys.: Conf. Ser.* 163, 012011 (2009).
27. P. Bogdanovich, R. Karpuškienė, A. Momkauskaitė, *Comput. Phys. Com.* 172, 133 (2005).
28. P. Bogdanovich, A. Momkauskaitė, *Comput. Phys. Commun.* 157, 217 (2004).
29. J. O. Ekberg, R. Kling and W. Mende, *Phys. Scr.* 61, 146 (2000).
30. H. Nilsson et al, *Eur. Phys. J. D* 49, 13 (2008).
31. R. Karpuškienė, P. Bogdanovich, O. Rancova, 41th EGAS Conference, Gdansk, 2009, Abstracts, p. 145.
32. R. Karpuškienė, P. Bogdanovich, O. Rancova, *J. Phys. B: At. Mol. Opt. Phys.* (submitted) (2009).
33. T. Pütterich et al., 31st Conference on Plasma Physics, London, ECA 28G, 4.136 (2004).
34. M. Stenke et al. *J. Phys. B: At. Mol. Opt. Phys.* 28, 4853, (1995).
35. V. Jonauskas, S. Kučas and R. Karazija. *Lithuanian Journal of Physics*, 2009.
36. M. F. Gu. *Astroph. J.* 582, 1241 (2003). 4th APS Topical Conference on Atomic Processes in Plasmas (AIP Proceedings vol. 730) Melville, N.Y.: AIP 2004.
37. Yu. Ralchenko, J. Reader, J. M. Pomeroy, J. N. Tan and J D Gillaspay. *J. Phys. B: At. Mol. Opt. Phys.* 40, 3861 (2007).
38. R. Karazija Introduction to the Theory of X-ray and Electronic Spectra of Free Atoms (New York: Plenum Press, 1996).
39. W.S.D. Loch et al. *Phys. Rev. A* 72, 052716 (2005).
40. D.-H. Kwon, Y.-J. Rhee, and Y.-K. Kim. *Int. J. Mass Spectrom.* 252, 213 (2006).
41. M. Stenke, et al. *J. Phys. B: At. Mol. Opt. Phys.* 28, 2711 (1995).
42. V. Jonauskas, S. Kučas and R. Karazija. 41st EGAS Conference Abstracts. Gdansk, 2009, p.156.
43. N.R. Badnell, *J. Phys. B*, 19, 3827 (1986).
44. N.R. Badnell, *J. Phys. B*, 30, 1 (1986).
45. R. Radtke, C. Biedermann, G. Fussmann, J. Schwob, P. Mandelbaum, R. Doron, *Atomic and Plasma - Material Interaction Data for Fusion* 13 45–66 (2007).
46. R. Radtke, C. Biedermann, P. Mandelbaum, J. L. Schwob, *Journal of Physics: Conference Series* 58 113–116 (2007).
47. C. F. Fischer, G. Gaigalas, Y. Ralchenko, *Computer Physics Communications* 175 (11-12) 738 – 744 (2006).
48. P. Jonsson, X. He, C. F. Fischer, I. Grant, *Computer Physics Communications* 177 (7) 597 – 622 (2007).
49. S. Kučas, V. Jonauskas, R. Karazija, *Physica Scripta* 55 (6) 667–675 (1997).
50. A. Kupliauskienė, V. Tutlys, *Nucl. Instr. Meth. Phys. Res. B*, 267, 263-265 (2009).
51. S. Kučas, R. Karazija, V. Jonauskas, and A. Momkauskaitė. *Phys. Rev.* (submitted).
52. A. Kupliauskienė, V. Tutlys. *Nucl. Instr. Meth. Phys. Res. B*, 267, 263 (2009).

ISSN 2029-1612



9 772029 161000